LASER GAIN SWITCHING TECHNIQUES AND CIRCUIT MODELLING

SEMICONDUCTOR LASER DIODE GAIN SWITCHING TECHNIQUES AND LASER DIODE EQUIVALENT CIRCUIT MODELLING IN SPICE

By

ROBERT BRUCE SZLAVIK, B.ENG. (SUMMA CUM LAUDE)

A Thesis

Submitted to the School of Graduate Studies

in Partial Fulfillment of the Requirements

for the Degree

Master of Engineering

McMaster University

MASTER OF ENGINEERING (1993) McMASTER UNIVERSITY
(Electrical and Computer Engineering) Hamilton, Ontario

TITLE: Semiconductor Laser Diode Gain Switching Techniques and Laser Diode Equivalent Circuit Modelling In SPICE

AUTHOR: Robert Bruce Szlavik, B.Eng. (McMaster University)

SUPERVISOR: Professor D.R. Conn

NUMBER OF PAGES: 125, xiv

Abstract

In developing a compact electro-optic sampling system for industrial use it is desirable to utilize a semiconductor laser diode as the light source since these devices are compact and economical. This thesis investigates several novel laser driver techniques for generating extremely short optical gain switched pulses from a semiconductor laser diode. These techniques include a novel bias control scheme in which the bias to a semiconductor laser diode, that is being driven with a step recovery diode pulse generator circuit, is turned on and off in order to switch the gain switched optical pulses on and off as desired. The second technique involves a mono-cycle scheme that allows a step recovery diode pulse generator circuit, which is customarily driven by a fixed frequency oscillator, to be driven by a mono-cycle pulse train of variable repetition rate. An equivalent circuit model of a laser diode based on the mono-mode rate equations is discussed and implemented in SPICE for the purpose of studying the interaction of the laser driver circuit electronics and the laser diode. The laser diode equivalent circuit is benchmarked against analytical solutions of the rate equations. A qualitative agreement between the measurements of the laser diode optical and terminal voltage responses and the SPICE simulations of the laser diode equivalent circuit model are demonstrated.

In Memory of my Grandfather

Andras Sudak
(1901-1990)

Acknowledgements

I would like to thank my supervisor Dr. D.R. Conn for his encouragement and support in all areas of my graduate studies at McMaster University. I would also like to thank my parents Mary and Paul Szlavik, without whose support this work would not have been possible.

I greatly appreciated the assistance of Mr. Kent Nickerson who was an excellent source of information and inspiration. I would like to thank Dr. S.H. Chisholm for his help. I would also like to acknowledge the technical staff in the Department of Electrical and Computer Engineering, specifically Mr. Ray Gillan and Mr. John Wells, for good practical advice. I would like to recognize my colleagues at the Communications Research Laboratory, specifically Dr. Jian Song, Xiahoua Wu and Junmei Zhang for their friendship.

I would also like to thank Bell Northern Research for funding the Electro-Optic Sampling System Project. In addition I would like to acknowledge the support of the Ontario Graduate Scholarship program.

Table of Contents

Table of Figures

Index of Symbols

$\mathbf{A}$	-	Area of laser active region perpendicular to direction of current flow (m^2)
α	-	Rate equations AC solution small signal constant (Hz)
α_1	-	Electron Fermi Dirac approximation constant (m^3)
α_2	-	Hole Fermi Dirac approximation constant (m^3)
β	-	Spontaneous recombination coupling coefficient (Dimensionless)
$\mathbf{c}$	-	Speed of light 3.0×10^{-8} (ms^{-1})
$\mathbf{C_{ph}}$	-	Laser diode model photon capacitance (F)
$\mathbf{C_1}$	-	Subcircuit 2.7 capacitance (F)
$\mathbf{D_1}$	-	Laser diode model terminal voltage (First) diode component
$\mathbf{D_2}$	-	Laser diode model terminal voltage (Second) diode component
$\mathbf{d}$	-	Width of the laser active region (m)
$\mathbf{E_A}$	-	Acceptor energy level (eV)
$\mathbf{E_c}$	-	Conduction band energy level (eV)
$\mathbf{E_{FEQ}}$	-	Equilibrium Fermi level (eV)
$\mathbf{E_{FN}}$	-	Equilibrium Fermi level n type AlGaAs (eV)
$\mathbf{E_{FP}}$	-	Equilibrium Fermi Level p type AlGaAs (eV)
$\mathbf{E_g}$	-	Active region energy band gap (eV)
$\mathbf{E_v}$	-	Valence band energy level (eV)
$\mathbf{F_n}$	-	Electron Quasi-Fermi level (eV)
$\mathbf{F_p}$	-	Hole Quasi-Fermi level (eV)
$\mathcal{F}_{1/2}$	-	Fermi Dirac integral abbreviation
$\mathbf{g_o}$	-	Optical gain constant (m^3/s)
$\mathbf{h}$	-	Plank's constant 6.63×10^{-34} (Js)
$\mathbf{I}$	-	Total laser diode terminal current (A)
$\mathbf{I_b}$	-	Gain switching initial DC bias current (A)
$\mathbf{I_{dc}}$	-	Steady state DC current component (A)
$\mathbf{I_e}$	-	Electrical current components of laser diode circuit model (A)
$\mathbf{I_g}$	-	Generic symbol for current (A)
$\mathbf{I_o}$	-	Total DC current component or initial inductor current (A)
$\mathbf{I_{spon}}$	-	Excess spontaneous recombination current (A)
$\mathbf{I_{stim}}$	-	Stimulated emission current component (A)
$\mathbf{I_{th}}$	-	Threshold current (A)
$\mathbf{I_{01}}$	-	Saturation current for junction voltage diode component D_1 (A)

I_{02} - Saturation current for junction voltage diode component D_2 (A)
ΔI - Small signal current component (A)
J_n - Electron current density (Am^{-2})
J_p - Hole current density (Am^{-2})
k - Boltzmann's constant 3.8×10^{-23} (J/K)
m - Gain switching solution slope of excess conduction band electron density $0 \leq t \leq t_o$ ($m^{-3}s$)
m_I - Input current modulation index (Dimensionless)
m_n - Excess conduction band electron density modulation index. (Dimensionless)
N - Total average conduction band electron density (m^{-3})
N_A - Acceptor concentration (m^{-3})
N_A^- - Ionized acceptor concentration (m^{-3})
N_c - Conduction band density of states (m^{-3})
N_o - Equilibrium conduction band electron density (m^{-3})
N_T - Total conduction band electron density (m^{-3})
N_v - Valence band density of states (m^{-3})
n - Excess conduction band electron density (m^{-3})
n_{dc} - Excess conduction band electron density DC component (m^{-3})
n_h - Gain switching solution excess conduction band electron density at half peak photon density (m^{-3})
n_{nmax} - Gain switching solution excess conduction band electron density peak value (m^{-3})
n_o - Gain switching excess conduction band electron density initial DC value (m^{-3})
n_{th} - Excess threshold conduction band electron density (m^{-3})
Δn - Excess conduction band electron density small signal component (m^{-3})
η_N - N-Type AlGaAs index of refraction
η_P - P-Type AlGaAs index of refraction
η_p - p-Type GaAs index of refraction
P - Total average valence band hole density (m^{-3})
P_o - Equilibrium Valence Band Hole Density (m^{-3})
p - Excess valence band hole density (m^{-3})
ϕ - Photon density (m^{-3})
ϕ_h - Gain switching solution half of peak photon density (m^{-3})
ϕ_{max} - Gain switching solution peak photon density (m^{-3})
ϕ_n - Photon density scaling constant (Dimensionless)
ϕ_{nmax} - Gain switching solution photon density at excess conduction band electron density peak (m^{-3})
ϕ_o - Gain Switching initial DC photon density (m^{-3})
ϕ_{nth} - Gain switching solution photon density at excess conduction band

		electron density threshold (m^{-3})
ϕ_{dc}	-	Steady state DC photon density component (m^{-3})
ϕ'	-	Laser diode model scaled photon density (m^{-3})
$\Delta\phi$	-	Small signal photon density component (m^{-3})
q	-	Electronic charge 1.6×10^{-19} (C)
R_{ph}	-	Laser diode model photon resistance (Ω)
R_s	-	Laser diode model series resistance (Ω)
R_1	-	Laser diode model terminal voltage resistive component (Ω)
R_2	-	Subcircuit 2.5 resistance (Ω)
T	-	Temperature in Kelvin (K)
t	-	Time (s)
t_h	-	Gain switching solution half peak photon density time (s)
t_o	-	Gain switching threshold excess conduction band electron density time (s)
t_p	-	Gain switching solution peak photon density time (s)
t_s	-	Gain switching solution excess conduction band electron density peak time (s)
T_1	-	Time interval of SRD cycle corresponding to the DC voltage level (s)
T_2	-	Time interval of SRD cycle corresponding to the pulse (s)
τ_{ns}	-	Combined excess spontaneous recombination time (s)
τ_{ph}	-	Photon lifetime (s)
Δt	-	Gain switching solution full width half maximum (s)
u	-	Gain switching solution excess conduction band electron density slope $t_s < t \leq t_p$ (s)
μ_p	-	Hole mobility ($m^2V^{-1}s^{-1}$)
μ_n	-	Electron mobility ($m^2V^{-1}s^{-1}$)
V	-	Generic symbol for voltage (V)
V_j	-	Laser diode model junction voltage (V)
V_T	-	Laser diode model terminal voltage (V)
V_{th}	-	Thermal voltage (kT)/q (V)
V_1	-	Voltage across R_1 laser diode junction voltage component (V)
V_2	-	Voltage across D_1 laser diode junction voltage component (V)
V_3	-	Voltage across D_2 laser diode junction voltage component (V)
υ	-	Light frequency (Hz)
w	-	Width of the laser diode active region (m)
ω_m	-	Input current modulation angular velocity (Hz)
ω_o	-	Rate equation AC solution resonance angular velocity (Hz)
ω_r	-	Resonance angular velocity of the SRD equivalent circuit corresponding to the time interval T_2 (Hz)
x	-	Spatial variable (m)
Ψ	-	Volume of the laser active region $A\times d$ (m^3)

ξ - Acceptor occupation probability approximation matching parameter (m^{-3})

Introduction

Discussion of the Problem

Electro-optic sampling is a promising measurement technique for high speed measurements of electronic circuitry. One of its principal features is that with an electro-optic sampling system, the circuit under test can be measured without actually having any physical contact between the circuit and the measuring instrument.

Electro-optic sampling systems use the electro-optic effect in which a beam of light pulses is passed through an electro-optic crystal which changes its optical properties under the influence of an electric field. The polarization of the light upon leaving the crystal is changed and this change is proportional to the intensity of the electric field in the crystal.

The light source in electro-optic sampling is an integral component in the overall system. Electro-optic sampling systems in use today exist primarily as research tools and these systems use large, expensive and complex commercial lasers as the light source. The commercial lasers that are used are capable of generating extremely short and

intense pulses of infra-red light with pulse widths on the order of 0.1 ps. Since the bandwidth of electro-optic sampling systems are inversely proportional to the pulse width of the light source, it is generally desired to have as narrow light pulses as practically possible.

In developing a compact electro-optic sampling system for industrial use, it is desirable to replace the traditional commercial laser with a more compact light source. The laser diode is a compact and inexpensive device that is relatively easy to use. In combination with laser driver microelectronics, the overall driver circuit can be made very small.

Semiconductor laser diodes, when gain switched, are capable of producing light pulses as narrow as 10 ps [1]. Gain switching refers to a mode of operation in which the laser diode is driven with large-amplitude but moderately fast electrical pulses. Due to nonlinear mechanisms in the laser, the optical pulses obtained are much shorter than the electric drive pulse. In effect, the first spike of a relaxation oscillation that appears during the transient turn on process is excited and the electrical pulse is terminated before the second relaxation oscillation spike appears [2]. Thus a semiconductor laser diode can be used to generate narrow optical pulses of suitable width for use in electro-optic sampling. Construction of a fixed pulse repetition rate gain switching laser driver circuit is straightforward. In designing a practical light source for electro-optic sampling systems, it is desirable to develop a laser driver that allows for a variable pulse repetition rate. The necessity for variable pulse repetition increases the complexity of the laser

driver circuit design.

An important parameter for optimization of the noise performance of electro-optic sampling systems is the timing jitter associated with the pulses from the light source. In terms of noise performance, it is desirable to keep the jitter of the light source as low as possible. A good parameter for evaluating the performance of perspective laser driver circuit techniques is to evaluate the laser driver jitter performance.

In order to evaluate perspective laser driver circuits for gain switching, it is desirable to have a model of the dynamic performance of the semiconductor laser diode that can be integrated with circuit simulation packages such as PSPICE. One advantage of such a model is that it can be used to simulate the interaction between the semiconductor laser diode and the components of the driver circuit electronics. If the model includes the dynamics of the photon density response to the electrical excitation, then the model can predict whether or not a particular laser driver circuit can be expected to gain switch the laser diode.

Review of Previous Work

Various different laser driver techniques have been utilized in the literature for the purpose of performing gain switching experiments. These techniques utilize electronic components that are capable of generating extremely short current pulses such

as step recovery diodes [3] and avalanche transistors [4]. In terms of timing jitter, the step recovery diode, or SRD, appears to be the device of choice [5].

A step recovery diode pulse generator is typically capable of producing current pulses of 300 mA into a 50 Ohm load with pulse widths under 100 ps. It can be shown experimentally, that these pulse widths are adequately short and the pulse amplitudes are sufficient to gain switch commercial semiconductor laser diodes with threshold currents of approximately 40 mA.

Laser diode equivalent circuit models have been reported in the literature by various authors [6], [7]. These circuit models are based on the mono-mode rate equations that describe the time rate of change of the excess conduction band electron density and the photon density in the active region of the semiconductor laser diode. To the author's knowledge, there has been no attempt reported in the literature to compare experimentally measured transient laser diode terminal voltages with laser diode equivalent circuit model simulations.

Scope of This Thesis

In this thesis project the experimental performance of various laser driver circuits for gain switching a semiconductor laser diode at variable pulse repetition rates are discussed. These techniques include a novel bias control scheme in which the bias to a semiconductor laser diode, that is being driven with an SRD, is turned on and off in

order to switch the gain switched pulses in and out. This laser driver circuit could be used in an electro-optic sampling system in which the step recovery diode oscillator is synchronized to the bias control signal on the laser driver circuit.

A second technique that is investigated is a mono-cycle scheme that allows the step recovery diode pulse generator circuit, which is customarily driven by a fixed frequency oscillator, to be driven by a mono-cycle pulse train of variable repetition rate. The effect of this mono-cycle driving scheme is to fire the step recovery diode pulse generator circuit, a pulse repetition frequency tuned device, at variable repetition rates. Such a laser driver technique could be used in an electro-optic sampling system as a pulse triggered laser driver circuit.

A simplified laser diode equivalent circuit model that incorporates some aspects of the circuit reported by Tucker [6] and the theoretical development by Jones [8] is discussed. The equivalent circuit model is implemented in PSPICE and the DC, small signal AC, and gain switched responses of the equivalent circuit model are benchmarked against the analytical solutions to the rate equations. It is demonstrated that for the gain switched response there is good agreement between the equivalent circuit model simulations and the analytical rate equations in terms of the gain switched pulse width prediction and the time delay between the onset of the electrical excitation pulse and the appearance of the first gain switched pulse.

The laser diode terminal voltage transient response predicted by the simulation of the step recovery diode pulse generator gain switching experiment agrees qualitatively

with the measured terminal voltage response. There is also a good agreement between the estimated widths of the measured gain switched optical pulses from the SRD experiment and the simulated optical pulse widths. It is also demonstrated that the characteristics of the optical response of the bias control SRD gain switched pulse switching circuit can be qualitatively simulated in PSPICE by simulating the circuit in conjunction with the laser diode equivalent circuit model.

This work can demonstrate a qualitative agreement between measured results and PSPICE simulations because the parameters for the laser diode equivalent circuit model that are used were taken from the literature. A quantitative agreement between the simulations and the measurements could only be verified by measuring the parameters of the semiconductor laser diodes that were used. Measurement of these parameters is beyond the scope of this work.

Chapter 1: Laser Diode Dynamic Response Modelling and the Rate Equations

To predict the dynamic response of semiconductor laser diodes, it is necessary to obtain the time response of the photon density ϕ in the lasing cavity in response to the electrical excitation current, I, injected into the device. The excitation current is intrinsically related to the excess conduction band electron density n through equation (1.1) and the dynamic response of the conduction band electron density is related to the dynamic response of the photon density ϕ through the two nonlinear coupled rate equations of (1.1) and (1.2).

$$\frac{dn}{dt} = \frac{I}{q\Psi} - \frac{n}{\tau_{ns}} - g_o n\phi \qquad (1.1)$$

$$\frac{d\phi}{dt} = g_o n\phi + \beta\frac{n}{\tau_{ns}} - \frac{\phi}{\tau_{ph}} \qquad (1.2)$$

The above nonlinear coupled laser diode rate equations describe the time variation of the photon density ϕ and the excess conduction band electron density n in the laser diode active region. An important assumption that is intrinsically implied by these rate

equations is that n and ϕ represent spatial average values of the excess conduction band electron density n and the photon density ϕ. Before discussing the details of the terms in equations (1.1) and (1.2) it is helpful to present a simplified physical diagram of a typical laser diode structure as shown in Fig 1.1.

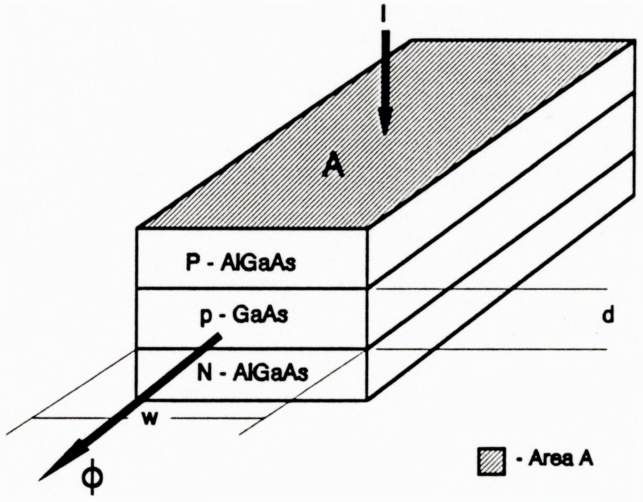

Figure 1.1 PpN Laser Diode Structure Simplified Diagram This diagram illustrates the positioning of the semiconductor regions in a PpN laser diode. The diagram also illustrates the direction of current flow I and the physical dimensions that represent the area of the active region A, the depth of the active region d and the width of the active region w. ϕ represents the light output.

Equation (1.1) defines the time rate of change of the excess conduction band electron density n. The $I/(q\Psi)$ term represents the injection of excess conduction band electrons from the excitation current I where q is the electronic charge, d is the width of the active region and A is the area of the active region perpendicular to the direction of the current flow I and $\Psi = A \times d$. This term is additive since current injection increases the excess conduction band electron density. The n/τ_{ns} term accounts for the excess conduction band electrons that recombine due to spontaneous recombination. A negative sign precedes this term since the spontaneous recombination depletes the excess conduction band electron density. The final term in equation (1.1) $g_o n\phi$ accounts for the recombination of excess conduction band electrons due to the stimulated emission where g_o is the optical gain constant. This term is preceded by a negative sign because the recombination due to stimulated emission depletes the excess conduction band electrons.

Equation (1.2) defines the time rate of change of the photon density ϕ in the active region of the laser diode. The first term $g_o n\phi$ accounts for the photons contributed from stimulated recombination. Since this term is additive, the sign of $g_o n\phi$ is positive. The $\beta n/\tau_{ns}$ term accounts for the fraction of photons that couple into the lasing mode from spontaneous emission. The last term ϕ/τ_{ph} models the photon losses in the cavity where τ_{ph} is the photon lifetime constant.

Three different solutions of the rate equations shown in (1.1) and (1.2) to three different types of excitation are discussed. The DC solution is presented first since it is the most straightforward. In verifying the accuracy of the laser diode equivalent circuit

model to be presented in chapter two, the analytically calculated DC solution is compared to the PSPICE simulated DC solution of the circuit model. The details of the DC excitation solution are also used in the derivation of the analytical gain switched solution presented at the end of this chapter. In addition to the DC excitation case, the AC excitation solution is presented in the second section of this chapter. The AC excitation case is also used to verify the accuracy of the simulated AC solution from the laser diode equivalent circuit model. The last analytical solution studied in section three of this chapter is the gain switched solution derived by Demokan [9]. This solution yields analytical expressions that define the principal characteristics of the gain switched pulses, these being the pulse width and the time delay between the electrical current pulse and the appearance of the gain switched optical pulse. For each of the three solutions discussed, the goal of this chapter is to derive analytical expressions relating the electrical excitation to the laser optical output.

1.1 The DC Excitation Case (The Steady State Solution)

Jones [8] outlines the solution to the rate equations for DC excitation. The highlights of this solution are outlined in this section along with an example of a simulated photon density versus DC excitation curve. The specific goal of this section is to develop an analytical expression that describes the functional dependence of the

steady state photon density ϕ_{dc} on the DC current.

Before proceeding with the highlights of the DC excitation solution it is necessary to establish a few basic definitions. The total conduction band electron density N is defined as the sum of the equilibrium conduction band electron density N_o and the excess conduction band electron density n. The thermal equilibrium situation is the condition that prevails if the semiconductor has been left unperturbed for an extended period of time [12]. The excess conduction band electron density n is defined as the sum of the excess steady state DC conduction band electron density n_{dc} and the small signal variation in the excess conduction band electron density Δn.

$$N_T = N_o + n = N_o + (n_{dc} + \Delta n) \tag{1.3}$$

A similar definition is adopted for the photon density. The photon density is defined to consist of a DC term ϕ_{dc} and a small signal term as shown in equation (1.4).

$$\phi = \phi_{dc} + \Delta\phi \tag{1.4}$$

It is convenient to define the current I as the sum of a DC component I_o and a small signal component ΔI. The DC component I_o can be further divided into two components, the first of which represents the DC current necessary to maintain the

threshold conduction band electron density when the photon density ϕ is zero and the second of which represents the additional DC current component required to sustain a steady state DC photon density ϕ_{dc}. The definition of I is stated mathematically in equation (1.5).

$$I = I_o + \Delta I = (I_{th} + I_{dc}) + \Delta I \tag{1.5}$$

In order to facilitate an analytical solution to the coupled nonlinear rate equations of (1.1) and (1.2) for the DC excitation case, the spontaneous emission coupling coefficient β is assumed to be equal to zero. The physical interpretation of this assumption is that no photons that are produced from spontaneous recombination couple into the lasing mode. The principal reason for making this assumption is to allow for an analytical solution to the coupled rate equations for the DC excitation case. The assumption of zero coupling coefficient in obtaining an analytical solution is valid since a very small fraction of the photons due to spontaneous emission couple into the lasing mode. A coupling coefficient of zero has been routinely assumed in the literature by various authors such as Jones [8] and Yariv [10] in deriving analytical solutions to the rate equations.

Before presenting the steady state or DC solution derivation, a definition of the steady state characteristics must be established. In this work the steady state will be

defined by (1.6) and (1.7).

$$\frac{dn}{dt} = 0 \qquad n \neq 0 \tag{1.6}$$

$$\frac{d\phi}{dt} = 0 \qquad \phi \neq 0 \tag{1.7}$$

The mathematical definition established by (1.6) and (1.7) define the steady state condition to be one in which the photon density does not change with time but is not equal to zero. The excess conduction band electron density does not change with time either but is not equal to zero under steady state conditions. It is clear that to be physically meaningful, neither the photon density nor the excess conduction band electron density can take on negative values.

Initially the photon density must build up from small values thus the condition necessary for the field in the laser cavity to build up is that

$$\frac{d\phi}{dt} \geq 0 \tag{1.8}$$

This condition of (1.8) applies so long as the photon density ϕ is small. As can be seen from equation (1.2), there are three cases regarding the time rate of change of the photon density that can be defined. The first case is defined by equation (1.8) and

describes the condition under which the photon density increases with time. There can also be a decreasing photon density with time in which case the time derivative of the photon density $(d\phi)/(dt)$ in (1.2) would take on a negative value. The third case is one in which the time rate of change of the photon density is equivalent to zero. This condition implies that the photon density is neither decreasing nor increasing with time.

$$n_{th} = \frac{1}{g_o \tau_{ph}} \tag{1.9}$$

Equation (1.2) can be solved for the excess conduction band electron density for the case in which the time rate of change of the photon density is equivalent to zero. This solution is presented in equation (1.9) and the value of the excess conduction band electron density for which the zero time rate of change of the photon density prevails is defined as the threshold excess conduction band electron density n_{th}. If the value of n is larger than n_{th} then the time rate of change of the photon density is positive and the photon density will increase with time. If n is smaller than n_{th} then the time rate of change of the photon density is negative and the photon density will decrease with time.

The value of n_{th} is the steady state value of the excess conduction band electron density since only when $n = n_{th}$ can $(d\phi)/(dt) = 0$ and $\phi \neq 0$ which are pre-requisite conditions for steady state as defined in (1.7). For any steady state value of the photon density ϕ, the excess conduction band electron density will be fixed at n_{th}. If the electron

density is fixed at n_{th} then it is implied that (dn)/(dt) = 0 and n $\neq$ 0.

It is necessary to define a threshold current I_{th} as the current required to maintain an excess conduction band electron density of n_{th} when the photon density is equal to zero. If zero is substituted into equation (1.1) for the photon density, n_{th} for the excess conduction band electron density and zero for the time rate of change of the excess conduction band electron density term (dn)/(dt) then equation (1.10) can be derived.

$$\frac{I_{th}}{q\Psi} = \frac{n_{th}}{\tau_{ns}} \qquad \textbf{(1.10)}$$

If equation (1.10) is re-substituted into equation (1.1) while still fixing the time rate of change of the excess conduction band electron density (dn)/(dt) equal to zero, the excess conduction band electron density equal to n_{th} and the photon density equal to a steady state value to be defined as ϕ_{dc} we can derive an expression for ϕ_{dc}.

$$\phi_{dc} = \frac{1}{g_o n_{th}}\left[\frac{I - I_{th}}{q\Psi}\right] \qquad \textbf{(1.11)}$$

Equation (1.11) describes the steady state photon density ϕ_{dc} as a function of the optical gain constant g_o, the threshold excess conduction band electron density n_{th}, the

electronic charge q, the width of the laser active region d and the area of the laser active region A that is perpendicular to the direction of current flow, the current required to sustain a threshold excess conduction band electron density I_{th} and the injected terminal current I.

The steady state photon density ϕ_{dc} versus the injected terminal current I is plotted in Fig. 1.2. This figure shows the light output versus electrical current relationship.

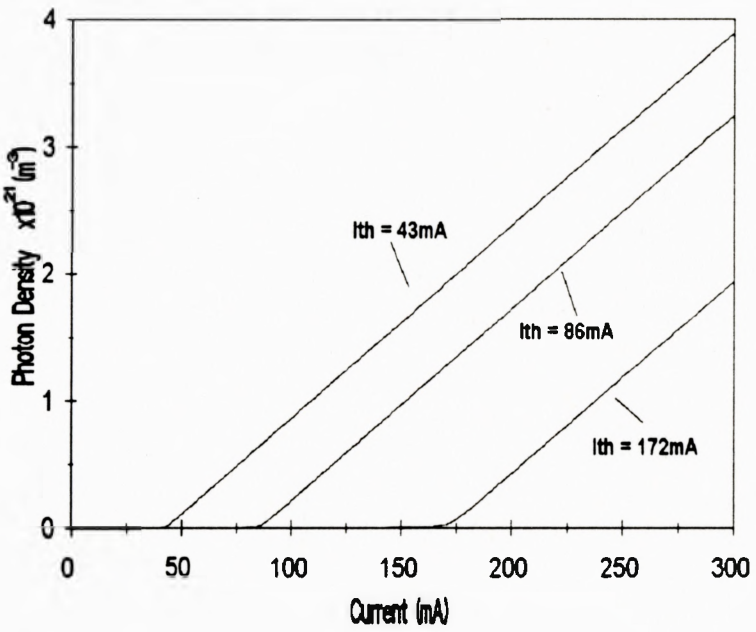

Figure 1.2 DC Photon Density Versus Terminal Current Characteristic for Three Lasers with Different Threshold Currents. Photon Density ϕ_{dc} (m^{-3}). Terminal Current I (mA).

Fig. 1.2 illustrates the DC output photon density versus DC input current for

three lasers with different threshold currents. From Fig 1.2 it can be seen that intensity modulation of the laser diode is best accomplished in the linear region where the device can be biased at a constant DC value with a small AC signal superimposed on the bias.

The excess conduction band electron density is plotted in Fig 1.3 below as a function of the injected terminal current I.

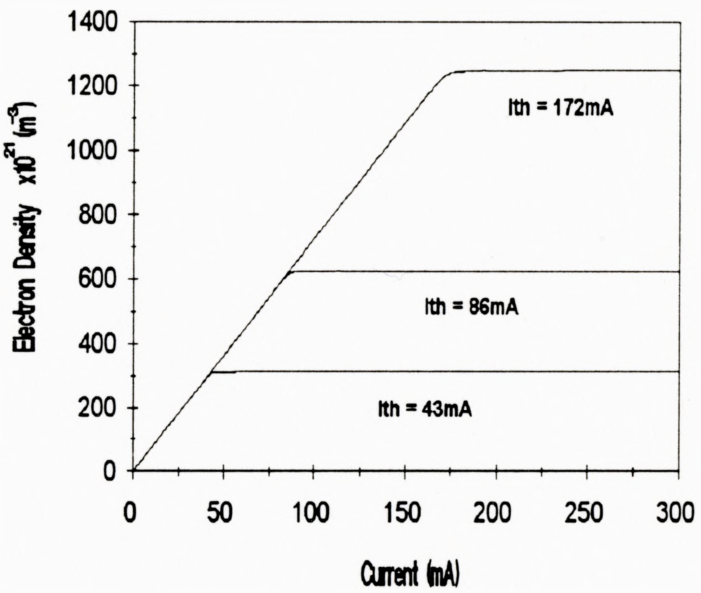

Figure 1.3 DC Excess Conduction Band Electron Density Versus Terminal Current Characteristic for Three Lasers with Different Threshold Currents. Excess Conduction Band Electron Density n (m^{-3}). Terminal Current I (mA).

Fig 1.3 graphically illustrates the saturation of the excess conduction band

electron density at the threshold value n_{th} for three lasers with different threshold currents. The excess conduction band electron density maintains the n_{th} value for steady state photon densities ϕ_{dc} greater than zero.

With the details of the DC steady state solution established it is now possible to proceed with a presentation of the AC excitation case.

1.2 The AC Excitation Case (Continuous Wave Intensity Modulation)

Jones [8] outlines the solution to the rate equations for AC excitation. The highlights of this solution are discussed in this section along with an example of the intensity frequency response. The goal of this section is to develop an expression for relating the intensity of the output light from the laser diode and the frequency of the driving current.

In order to proceed with the solution to the AC excitation case, it is necessary to derive the small signal rate equations. This derivation is accomplished by substituting the expression for the excess electron density, including both the DC and small signal terms into the electron density rate equation of (1.1). Since it is assumed that the laser diode is biased in the linear region of the photon density versus injected current curve of Fig. 1.2, the DC component of the excess conduction band electron density is assumed to be equal to the threshold value n_{th} since the laser is biased above threshold.

$$n = n_{th} + \Delta n \tag{1.12}$$

The photon density ϕ is also replaced with its steady state DC component and the small signal component.

$$\phi = \phi_{dc} + \Delta\phi \tag{1.13}$$

The excitation current I is also assumed to consist of the DC and AC small signal components as per equation (1.5).

Equation (1.13) is substituted into rate equation (1.2) that governs that time rate of change of the photon density. It is assumed once again that there is no coupling of the spontaneous emission into the lasing mode or that β is equal to zero. This assumption is made to simplify the AC solution. Terms that contain the $\Delta n \Delta\phi$ product are assumed to be negligibly small and are omitted.

Substituting (1.12) and (1.13) into equation (1.1) and (1.2) and cancelling equivalent terms yields the following small signal rate equations of (1.14) and (1.15).

$$\frac{d\Delta n}{dt} = \frac{\Delta I}{q\Psi} - \frac{\Delta n}{\tau_{ns}} - g_o \Delta n \phi_{dc} - g_o \Delta\phi n_{th} \tag{1.14}$$

$$\frac{d\Delta\phi}{dt} = g_o \Delta n \phi_{dc} \tag{1.15}$$

If the small signal excess electron density equation of (1.14) is differentiated with respect to time, then the term containing $\Delta\phi$ can eliminated yielding a single differential

equation that is in terms of only the Δn variable.

$$\frac{d^2\Delta n}{dt^2} = \frac{1}{q\Psi}\frac{d\Delta I}{dt} - \left[\frac{1}{\tau_{ns}} + g_o\phi_{dc}\right]\frac{d\Delta n}{dt} - g_o^2 n_{th}\phi_{dc}\Delta n \qquad (1.16)$$

The following substitutions are made in order to simplify equation (1.16).

$$2\alpha = g_o\phi_{dc} + \frac{1}{\tau_{ns}} \qquad (1.17)$$

$$\omega_o^2 = g_o^2 n_{th}\phi_{dc} \qquad (1.18)$$

Equation (1.16) is rewritten in equation (1.19) in a simplified form using the substitution from (1.17) and (1.18).

$$\frac{d^2\Delta n}{dt^2} + 2\alpha\frac{d\Delta n}{dt} + \omega_o^2\Delta n = \frac{1}{q\Psi}\frac{d\Delta I}{dt} \qquad (1.19)$$

Sinusoidal modulation of the input current I is assumed with the goal being to calculate the response of the small signal photon density as a function of time $\Delta\phi(t,\omega_m)$. The functional form of the current I is shown in equation (1.20) where m_f is referred to as the modulation index of the input current ω_m is the modulation angular velocity.

$$I = I_o\left[1 + m_f e^{j\omega_m t}\right] \qquad (1.20)$$

The term on the right hand side of equation (1.19) containing the derivative of ΔI

can be derived using (1.20).

$$\frac{1}{q\Psi}\frac{d\Delta I}{dt} = jI_o m_I e^{j\omega_m t} \tag{1.21}$$

The particular solution of the differential equation shown in (1.19) is shown in (1.22) where m_n is the modulation index of the excess conduction band electron density.

$$n = n_{th}\left[1 + m_n e^{j\omega_m t}\right] \tag{1.22}$$

In the AC small signal solution to the rate equations we are only interested in the small signal portion of the above solution.

$$\Delta n = n_{th} m_n e^{j\omega_m t} \tag{1.23}$$

If the small signal component of the excess conduction band electron density, shown in (1.23), is substituted back into the differential equation of (1.19), an expression for the excess conduction band electron density modulation index m_n can be derived as shown in (1.24).

$$m_n = j\frac{I_o m_I \omega_m}{q\Psi n_{th}}\frac{1}{\left(\omega_o^2 - \omega_m^2\right) + j2\alpha\omega_m} \tag{1.24}$$

In order to derive an expression for $\Delta\phi(t,\omega_m)$ the excess small signal conduction band electron density can be substituted into the small signal rate equation governing the

photon density of equation (1.15). Solving equation (1.15) then yields the expression of (1.25).

$$\Delta\phi(t,\omega_m) = \frac{g_o\phi_{dc}m_n n_{th}e^{j\omega_m t}}{j\omega_m} \tag{1.25}$$

Substituting in the expression for the modulation index for the excess conduction band electrons m_n of equation (1.24) and rearranging makes it possible to rewrite $\Delta\phi(t,\omega_m)$.

$$\Delta\phi(t,\omega_m) = \frac{g_o\phi_{dc}I_o m_I}{q\Psi\omega_o^2}\frac{e^{j\omega_m t}}{\left(1 - \frac{\omega_m^2}{\omega_o^2}\right) + j\frac{2\alpha\omega_m}{\omega_o^2}} \tag{1.26}$$

We can identify a factor $M(\omega_m)$ from equation (1.26) which defines the relationship between the intensity of the output light from the laser diode and the frequency of the driving current.

$$M(\omega_m) = \frac{1}{\left(1 - \frac{\omega_m^2}{\omega_o^2}\right) + j\frac{2\alpha\omega_m}{\omega_o^2}} \tag{1.27}$$

Equation (1.27) is the principal expression of this section in that it defines the frequency response of the optical intensity emitted from the laser diode.

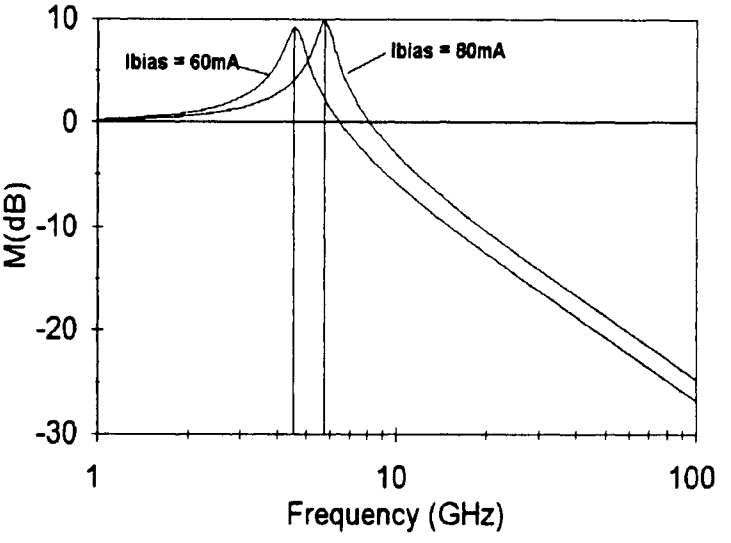

Figure 1.4 M(dB) Versus Frequency Curve for AC Excitation of an I_{th}=43 mA Laser at Two Different DC Bias Levels This curve relates the light intensity emitted from the laser diode to the frequency of the excitation current. Frequency is in units of (GHz) and M, as defined in equation (1.27) is in units of (dB).

Fig. 1.4 illustrates the optical output of a laser diode as a function of the input current frequency. When the angular velocity of the current ω_m is equal to ω_o defined in equation (1.18) the photon density versus frequency curve of Fig. 1.4 reaches a resonance peak. The angular velocity ω_o corresponds to the frequency at which their is

a resonance between the energy contained in the photons of the field and the energy contained in the electrons of the conduction band.

In practical systems that rely on modulation of the light intensity, the maximum modulation frequency of the input current must be limited to approximately half the frequency of the resonance peak in order to avoid distortion in the waveform.

1.3 The Gain Switched Solution

This section focuses on developing analytical expressions that describe the principal characteristics of the laser diode gain switched response. In this section analytical expressions are developed for the time delay between initiation of the electrical current pulse and the appearance of the gain switched optical pulse as well as the optical pulse width.

Throughout this section it is necessary to refer to various features of the photon density versus time curve $\phi(t)$ and the excess conduction band electron density versus time curve n(t). Fig. 1.5 identifies the important features of $\phi(t)$ and n(t).

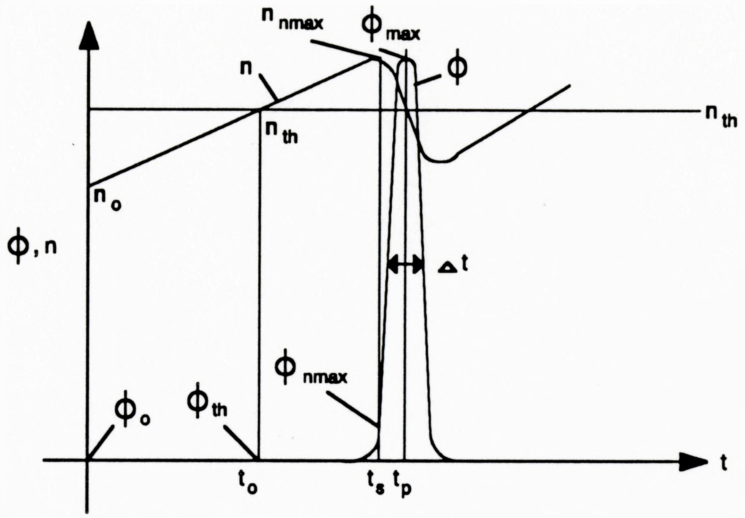

Figure 1.5 Gain Switched Response of Excess Conduction Band Electron Density n And Photon Density ϕ. n_o - Initial Excess Conduction Band Electron Density (m^{-3}). n_{th}- Threshold Excess Conduction Band Electron Density (m^{-3}). n_{nmax} - Maximum Excess Conduction Band Electron Density (m^{-3}). ϕ_o - Initial Photon Density (m^{-3}). ϕ_{nth} - Photon Density at Excess Conduction Band Electron Density Threshold Value (m^{-3}). ϕ_{nmax} - Photon Density at Maximum Excess Conduction Band Electron Density (m^{-3}). ϕ_{max} - Maximum Photon Density(m^{-3}). Δt - Gain Switched Pulse Width (s). t_o - Threshold Excess Conduction Band Electron Density Time (s). t_s - Maximum Excess Conduction Band Electron Density Time (s). t_p - Peak Photon Density Time (s).

The functional form of the excitation current pulse used to gain switch the laser diode is shown in Fig. 1.6.

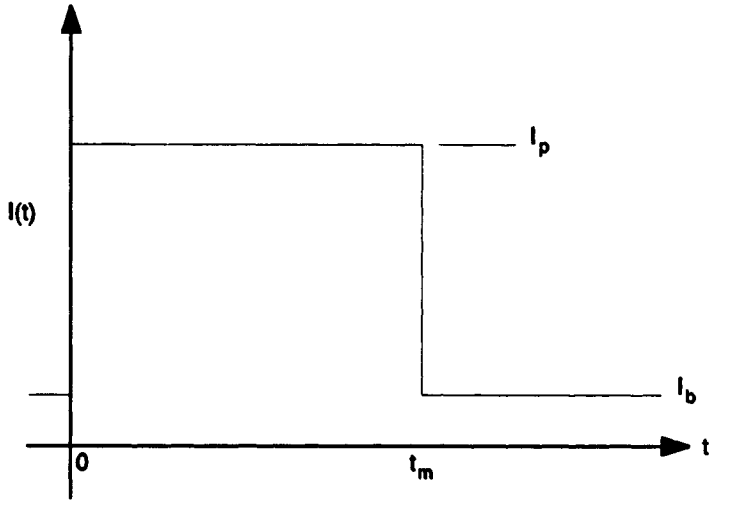

Figure 1.6 Functional Form of the Input Current I Versus Time I(t) - Current (Amps) t - Time (s).

Before time zero, the current level is assumed to be maintained at I_b which is just below threshold. At t = 0 the current is stepped to a value I_p that is approximately five times the threshold current of the laser diode. At a time t_m, the current level steps back down to I_b. The time t_m occurs after t_p in Fig. 1.5. Typically t_m is 100 ps. If t_m is made too long, a series of optical relaxation oscillations will appear. The time t_m must be chosen such that the current pulse is cutoff before the second oscillation spike appears.

Demokan [9] presents a solution to the rate equations for the gain switched response. We begin with the rate equations as presented in equations (1.1) and (1.2). An initial bias current I_b that is below the threshold current I_{th} is applied to the laser

diode. The expression for the initial photon density ϕ_o is arrived at by assuming that up until the first current pulse steady state DC conditions have prevailed and the conduction band electron density is and has been maintained at a value of n_o which is below n_{th}.

The analysis begins with the equation defining the time rate of change of the photon density as shown in (1.2). The photon density takes on a DC steady state initial value that is defined as ϕ_o. This initial photon density comes from spontaneous emission that couples into the lasing mode. The stimulated emission term in equation (1.2) is set to zero however unlike the DC solution outlined in the first section of this chapter, the spontaneous emission coupling coefficient β is not zero. Since there is no time rate of change of the photon density under DC steady state conditions, the time derivative term in equation (1.2) is set to zero. As a consequence of these conditions, an expression for the DC steady state photon density value ϕ_o can be written.

$$\phi_o = \beta n_o \frac{\tau_{ph}}{\tau_{ns}} \tag{1.28}$$

Under steady state conditions, the excess conduction band electron density does not vary with time maintaining a DC value of n_o. Since the excess conduction band electron density maintains a steady state value, the time derivative in equation (1.1) is set to zero. The stimulated emission term is also set to zero since the excess conduction band electron density is below the threshold value and thus the stimulated emission is assumed to be negligible. Using the conditions discussed above, equation (1.1) can be

solved for the initial excess conduction band electron density n_o.

$$n_o = \frac{I_b \tau_{ns}}{q\Psi} \tag{1.29}$$

If the initial bias current is chosen such that $I_b > I_{th}$ then the spontaneous emission term in the photon density rate equation of (1.2) can be neglected since stimulated emission dominates. Since steady state conditions are assumed initially, the photon density does not change with time maintaining a DC value. This condition implies that the time rate of change of the photon density term is zero in equation (1.2). Since the initial bias current is greater than the current necessary to maintain a threshold conduction band electron density, stimulated emission dominates and the excess conduction band electron density is clamped at the threshold value n_{th} as explained earlier in this chapter. The expression for the threshold excess conduction band electron density is given in (1.9).

$$n_{th} = \frac{1}{\tau_{ph} g_o} \tag{1.30}$$

An expression for the initial photon density ϕ_o under the $I_b > I_{th}$ DC excitation condition can be derived from the excess conduction band electron density rate equation of (1.1) as was shown earlier yielding equation (1.11).

$$\phi_o = \tau_{ph}\left[\frac{I_b}{q\Psi} - \frac{n_{th}}{\tau_{ns}}\right] \tag{1.31}$$

Having presented Fig. 1.5, it is now possible to discuss the functional form of the excess conduction band electron density n and the photon density ϕ in the gain switching solution during the time interval $0 < t < t_o$. Since the conduction band electron density remains below n_{th}, the stimulated emission term in the conduction band electron density rate equation is negligible. The electron density rate equation thus reduces to the form shown in equation (1.32).

$$\frac{dn}{dt} = \frac{I(t)}{q\Psi} - \frac{n}{\tau_{ns}} \tag{1.32}$$

The contribution of the spontaneous emission term n/τ_{ns} is small and can be replaced with the constant term n_{th}/τ_{ns} as per Demokan [9]. Making this replacement allows equation (1.32) to be written as shown in (1.33).

$$\frac{dn}{dt} = \frac{I(t)}{q\Psi} - \frac{n_{th}}{\tau_{ns}} \tag{1.33}$$

The photon density rate equation of (1.2) can also be simplified since there is negligible stimulated emission and the stimulated emission term can be neglected. The photon density is assumed to be very small since the conduction band electron density remains below threshold during this time interval. Because the photon density is small,

the term ϕ/τ_{ph} that models the photon losses in the lasing cavity can also be neglected. Equation (1.2) can thus be simplified to the form shown in (1.34).

$$\frac{d\phi}{dt} = \beta\frac{n}{\tau_{ns}} \tag{1.34}$$

Equation (1.33) can be solved for the functional form of the excess conduction band electron density shown in (1.35).

$$n = mt + n_o \tag{1.35}$$

The excess conduction band electron density equation of (1.35) is a straight line which implies that in this region, the excess conduction band electron density increases linearly with time. The m coefficient in (1.35) is simply the slope of the straight line and is equivalent to the time rate of change of the electron density as written in (1.32).

$$m = \frac{I(t)}{q\Psi} - \frac{n_{th}}{\tau_{ns}} \tag{1.36}$$

The solution of (1.35) can be substituted into the simplified photon density rate equation of (1.34).

$$\frac{d\phi}{dt} = \frac{\beta}{\tau_{ns}}[mt + n_o] \tag{1.37}$$

The solution to the above photon density rate equation is shown in (1.38).

$$\phi = \frac{\beta t}{\tau_{ns}}\left[\frac{mt}{2} + n_o\right] + \phi_o \qquad (1.38)$$

At time $t = t_o$ the excess conduction band electron density reaches the threshold value n_{th} as per Fig. 1.5. The photon density at time t_o can be found by substituting the time t_o into equation (1.38).

$$\phi_{nth} = \frac{\beta t_o}{\tau_{ns}}\left[\frac{mt_o}{2} + n_o\right] + \phi_o \qquad (1.39)$$

Since the excess conduction band electron density, as a function of time, is linear during the time interval $0 \succ t \succ t_o$, the time t_o can be solved for using equation (1.35) by substituting in the threshold value of the excess conduction band electron density for n since at time t_o the excess conduction band electron density is equivalent to the threshold value n_{th}.

$$t_o = \frac{n_{th} - n_o}{m} \qquad (1.40)$$

Having derived expressions for the excess conduction band electron density, photon density and time t_o it is now possible to proceed to an examination of the next time interval which is $t_o \succ t \succeq t_s$ as per Fig. 1.5. During this time interval the excess conduction band electron density is greater than the threshold value n_{th} therefore stimulated emission dominates in the photon density rate equation which must be rewritten as in (1.41).

$$\frac{d\phi}{dt} = g_o(n - n_{th})\phi \tag{1.41}$$

The excess conduction band electron density is continuous across the boundary between the time intervals of $0 \geq t \geq t_o$ and $t_o > t \geq t_s$ and maintains the functional form of a straight line with the same slope as in the previous time interval as per Demokan [9]. Equation (1.42) is an expression of the functional form of the excess conduction band electron density in the $t_o > t \geq t_s$ time interval.

$$n = m(t - t_o) + n_{th} \tag{1.42}$$

The above expression for n can be substituted into the modified photon density rate equation of (1.41) for the purpose of solving for the functional form of ϕ which is given in (1.43).

$$\phi = \phi_{nth} e^{\frac{g_o m}{2}(t - t_o)^2} \tag{1.43}$$

At time $t = t_s$, the excess conduction band electron density reaches its maximum value and the photon density will take on a specific numerical value that we will specify as $\phi = \phi_{nmax}$.

$$\phi_{nmax} = \phi_{nth} e^{\frac{g_o m}{2}(t_s - t_o)^2} \tag{1.44}$$

In order to solve for n_{nmax}, another expression for ϕ_{nmax} is needed. The other required equation is shown in (1.45) and can be derived from the excess conduction band electron density rate equation of (1.1). When the excess conduction band electron density reaches it maximum value, the function will have zero slope and therefore the time derivative term in (1.1) will be zero. If the value for n_{nmax} is substituted into equation (1.1) then an expression can be derived for the value of the photon density at time t_s when the excess conduction band electron density is at its maximum value.

$$\phi_{nmax} = \frac{\frac{I(t)}{q\Psi} - \frac{n_{nmax}}{\tau_{ns}}}{g_o n_{nmax}} \tag{1.45}$$

Since the excess conduction band electron density function is linear in this region, as can be seen from (1.42), we can substitute the maximum excess conduction band electron density value into equation (1.42) and solve for the time t_s.

$$t_s = t_o + \frac{n_{nmax} - n_{th}}{m} \tag{1.46}$$

This equation allows us to recast the first equation derived for the photon density at time t_s of (1.44) in terms of the maximum and threshold excess conduction band electron density n_{nmax}, n_{th} and the slope of the excess conduction band electron density

function m instead of the time variables t_s and t_o.

$$\Phi_{nmax} = \Phi_{nth} e^{\frac{g_o}{2m}(n_{nmax} - n_{th})^2} \tag{1.47}$$

The reason for deriving two equations for ϕ_{nmax} in terms of n_{nmax} is that equations (1.47) and (1.45) can be equated and n_{nmax} can be solved for numerically.

$$n_{nmax} - n_{th} = \sqrt{\frac{2m}{g_o} \ln\left[\frac{\frac{I(t)}{q\Psi} - \frac{n_{nmax}}{\tau_{ns}}}{\Phi_{nth} g_o n_{nmax}}\right]} \tag{1.48}$$

The next time interval that will be considered, as per Fig. 1.5, is the time between the peak excess conduction band electron density and the peak photon density. Defined mathematically, this time interval is $t_s < t \leq t_p$. In this region, the excess conduction band electron density can be approximated by a straight line with a negative slope of magnitude u as per Demokan [9].

$$n = n_{nmax} - u(t - t_s) \tag{1.49}$$

Since the excess conduction band electron density in this time interval is above the threshold value, the photon density rate equation, as presented for the previous time interval in equation (1.41), can be used for the present time interval under study. If the equation for the excess conduction band electron density in this time interval is

substituted into (1.41) a new photon density rate equation can be derived.

$$\frac{d\phi}{dt} = g_o[n_{nmax} - u(t - t_s) - n_{th}]\phi \qquad \textbf{(1.50)}$$

The solution to the above rate equation of (1.50) is

$$\phi = \phi_{nmax} e^{\left[n_{nmax}g_o(t - t_s) - n_{th}g_o(t - t_s) - \frac{u}{2}g_o(t - t_s)^2\right]} \qquad \textbf{(1.51)}$$

The modified photon density rate equation of (1.50) can be used to solve for the time t_p at which the photon density reaches its maximum value of ϕ_{max}. This solution is derived by noting that at the maximum photon density, the time rate of change term in (1.50) will be zero and t_p can be solved for directly.

$$t_p = \frac{n_{nmax} - n_{th}}{u} + t_s \qquad \textbf{(1.52)}$$

An expression for the maximum photon density ϕ_{max} can be written by substituting $t_p - t_s$ from (1.52) into the solution of the photon density rate equation for this time interval.

$$\phi_{max} = \phi_{nmax} e^{\frac{g_o}{2u}(n_{nmax} - n_{th})^2} \qquad \textbf{(1.53)}$$

In order to develop an expression for the gain switched full width half maximum (FWHM) pulse width, equation (1.53) must be used to derive an expression for half of

the maximum peak value of the photon density.

$$\phi_h = \frac{\phi_{nmax}}{2} e^{\frac{g_o}{2u}(n_{nmax} - n_{th})^2} \tag{1.54}$$

In equation (1.49) an expression was written for the functional form of the excess conduction band electron density during this time interval. The value of the excess conduction band electron density at time t_h, when the photon density first reaches half of its peak value, will be denoted by n_h.

$$t_h - t_s = \frac{n_{nmax} - n_h}{u} \tag{1.55}$$

The above expression for $t_h - t_s$ can be substituted into the general expression for the photon density of (1.51) derived for this time interval and equated to the half maximum expression for the photon density of equation (1.54).

$$\frac{1}{2} e^{\frac{g_o}{2u}\left(n_{nmax}^2 - 2n_{nmax}n_{th} + n_{th}^2\right)} = e^{g_o\left[\frac{n_{nmax} - n_h}{u}\right]\left[n_{nmax} - n_{th} - \frac{1}{2}(n_{nmax} - n_h)\right]} \tag{1.56}$$

After some simplification, equation (1.56) can be simplified to an equivalent form shown below in equation (1.57).

$$n_h - n_{th} = \sqrt{\frac{2uln2}{g_o}} \tag{1.57}$$

It should be noted from Fig. 1.5 that as the photon density increases in magnitude, the excess conduction band electron density decreases from its maximum value of n_{nmax}. When the excess conduction band electron density reaches the threshold value of n_{th} the photon density reaches its maximum value of ϕ_{max}. The physical reason for this phenomenon is that once the electron threshold value is reached, there are no further excess conduction band electrons available to contribute to the stimulated emission, thus the photon density pulse amplitude can increase no further.

If n_{th} is subtracted from both sides of equation (1.55) then an expression for $n_h - n_{th}$ can be written.

$$n_h - n_{th} = u(t_p - t_s) - u(t_h - t_s) \tag{1.58}$$

Substituting (1.58) into equation (1.57) allows us to write an expression for half of the full width half maximum pulse width.

$$t_p - t_h = \sqrt{\frac{2ln2}{g_o u}} \tag{1.59}$$

The equation for the full width half maximum pulse width Δt is simply (1.59) with both sides of the equation multiplied by two.

$$\Delta t = \sqrt{\frac{8\ln 2}{g_o u}} \tag{1.60}$$

The value of the slope of the excess conduction band electron density u during this time interval is still an unknown quantity. An implicit expression for u can be found by using the rate equations for the excess conduction band electron density and the photon density as presented in (1.1) and (1.41) respectively.

At time t_p, when the photon density reaches its maximum value, the slope of the photon density function will be zero and time rate of change term in equation (1.41) can be set to zero. An expression for the excess conduction band electron density can be solved for directly yielding the expression for n shown in (1.61).

$$n = n_{th} \tag{1.61}$$

The result of (1.61) is of no surprise since the photon density can only increase so long as the excess conduction band electron density remains above the threshold value. At time t_p, the photon density is at its maximum value of ϕ_{max} as was discussed earlier. During this time interval the excess conduction band electron density maintains a slope of -u. The time derivative term in the excess conduction band electron density rate equation of (1.1) can thus be replaced with -u. An alternate expression for the maximum photon density ϕ_{max} can be written.

$$\phi_{max} = \tau_{ph}\left[\frac{I(t)}{q\Psi} - \frac{n_{th}}{\tau_{ns}} + u\right] \qquad (1.62)$$

The two expressions for the peak photon density of (1.53) and (1.62) can be equated yielding an implicit equation for u that can be solved for numerically using equation (1.63)

$$u = \frac{g_o(n_{nmax} - n_{th})^2}{2\ln\left[\frac{\tau_{ph}}{\phi_{nmax}}\left(\frac{I(t)}{q\Psi} - \frac{n_{th}}{\tau_{ns}} + u\right)\right]} \qquad (1.63)$$

The analytical equation for the full width half maximum pulse width of (1.60) describes one of the principal observable characteristics of a gain switched pulse of interest. Assuming that the parameters of a semiconductor laser diode are known, these two equations can be used to predict the width of the gain switched pulse. The equation that quantifies the peak photon density time t_p can also be used to predict the time between the initiation of the excitation current pulse and the appearance of the gain switched optical pulse.

In this chapter, the solutions to the laser diode rate equations have been presented for the DC, small signal AC and the gain switched pulsed excitation conditions. In chapter two, a laser diode equivalent circuit model will be described along with the

implementation of the equivalent circuit model in PSPICE. In subsequent chapters, the principal equations that were derived in this chapter that describe the time response of the photon density for DC, AC and gain switched excitations will be used as a benchmark to evaluate the accuracy of the laser diode equivalent circuit model.

Chapter 2: Laser Diode Equivalent Circuit Model

The goal of this chapter is to derive an equivalent circuit model for a laser diode that can be implemented in PSPICE and that predicts the terminal voltage V_T as well as the light output ϕ'. The derivation is a combination of the rate equations presented in chapter one and the work of Tucker [14]. Fig. 2.1 shows the equivalent circuit model that emerges from the derivation.

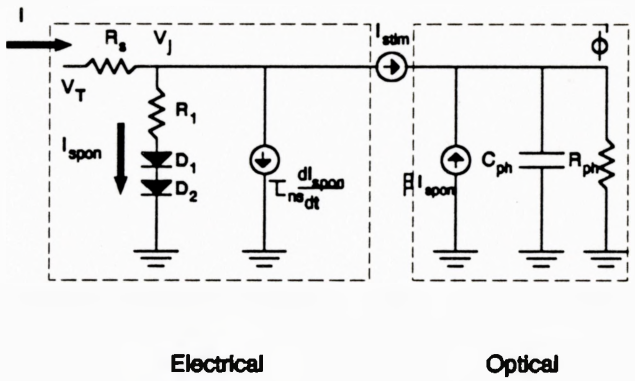

Figure 2.1 Laser Diode Equivalent Circuit Model V_T - Terminal Voltage. ϕ' -Scaled Photon Density (Voltage). R_s - Laser Diode Series Resistance. C_{ph} - Photon Capacitance (Photon Time Rate of Change Term). R_{ph} - Photon Resistance (Photon Cavity Loss Term). R_1, D_1, D_2 - Terminal Voltage Components. Current sources from left to right model time rate of change of conduction band electron density (charge storage effect) $\tau_{ns}d(I_{spon})/(dt)$, stimulated emission current component I_{stim} and the spontaneous recombination coupling photon source βI_{spon}.

This circuit can be divided into two halves. The first half models the electrical characteristics of the device and the second half models the light output of the laser. The electrical and optical halves of the circuit are coupled to each other through the nonlinear current source that models the stimulated emission I_{stim}.

On the electrical side, it is necessary to account for the current due to excess spontaneous recombination. The excess spontaneous recombination current, which is proportional to the excess conduction band electron density n, is the current drawn by the series junction components R_1, D_1 and D_2 in the laser diode equivalent circuit model. It is also necessary to account for the time rate of change of the charge storage as a current component which is proportional to the time rate of change of the conduction band electron density in the rate equations. This current component is modelled by the $\tau_{ns}(dI_{spon})/(dt)$ current source in the laser diode equivalent circuit model. Current lost to stimulated emission must also be accounted for and this is done through the nonlinear controlled current source I_{stim}. The total current into the terminals of the laser diode equivalent circuit is the sum of the current components discussed above. It should be noted at this time that all these current components can be written in terms of the excess spontaneous recombination current that is proportional to n as shown in equation (2.1).

$$I_{spon} = \frac{qn\Psi}{\tau_{ns}} \qquad (2.1)$$

To obtain an electrical current voltage characteristic of the laser diode, the current into the device must be related to the voltage across the laser. The expression for the junction voltage V_j must also be of a form that facilitates implementation in PSPICE. It is shown that suitable expressions for the components of the junction voltage can be written in terms of the excess spontaneous recombination current that is proportional to n. The junction voltage components are accounted for by the resistance R_1 and the two diode components D_1 and D_2 in the laser diode equivalent circuit model.

The photons contributed from stimulated emission are modelled by the nonlinear current source I_{stim}. Photon losses in the laser cavity are accounted for through the resistance R_{ph} in the laser diode equivalent circuit model. The time rate of change of the photon density in the rate equations is accounted for by the C_{ph} capacitance component in the equivalent circuit model. There is also a component of spontaneous emission that couples into the lasing mode and this effect is accounted for by the current source βI_{spon}.

The excess spontaneous recombination current I_{spon} that is proportional to n provides the link between the junction voltage expressions and the current that the laser diode equivalent circuit model draws since all the junction voltage expressions and the current components are written in terms of this quantity.

Derivations of mathematical expressions for the electrical current components and junction voltage components of the laser diode equivalent circuit model are based on the work of Tucker [14] and are discussed in the following sections of the chapter. The stimulated emission current component as well as the components in the optical half of

the laser diode equivalent circuit are also derived. A discussion of the implementation details of the equivalent circuit model in PSPICE is presented.

Before proceeding with the derivation of the electrical characteristics of the laser diode equivalent circuit model, it is first necessary to introduce the energy band diagram of the device since much of the discussion that follows relies on terms and concepts that relate to the energy band diagram.

2.1 Energy Band Diagram of Double Heterojunction Laser Diodes

From a device structure perspective, a laser diode can be constructed as a simple pn junction. The energy band diagram of a simple pn junction laser is similar to a conventional pn junction diode energy band diagram as discussed in Streetman [11]. A principal drawback of a simple pn junction laser diode structure is that there is nothing inherent in the structure of the device that confines the carriers to the region where the carrier recombination takes place, hereafter referred to as the active region. This limitation results in higher threshold currents than would otherwise be necessary with more advanced device structures. One such advanced structure is the double heterojunction laser diode and the principal advantages of this structure, as outlined by Jones [8], are:

1. A double heterojunction device will have a lower threshold current than a single heterojunction device or an ordinary pn diode structure. The increase in carrier

confinement is a result of the fact that the carriers in the double heterojunction are confined to the active p region which results in a population inversion sufficient to induce stimulated emission at lower current levels than would otherwise be possible.

2. The double heterostructure provides a physical confinement of the optical wave. This confinement is due to the differences in the index of refraction between the active region and the regions surrounding it which provides a natural planar waveguide.

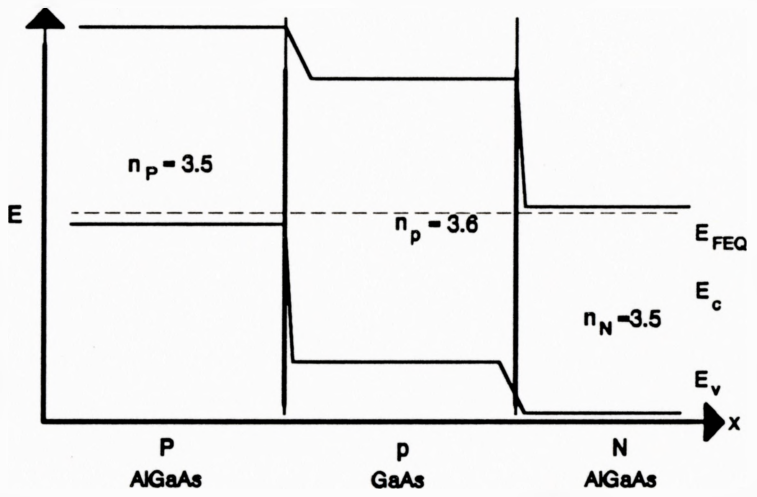

Figure 2.2 PpN Laser Diode Energy Band Diagram at Equilibrium η_P - P AlGaAs Index of Refraction. η_p - p GaAs Index of Refraction. η_N - N AlGaAs Index of Refraction. E_{FEQ} - Equilibrium Fermi Level

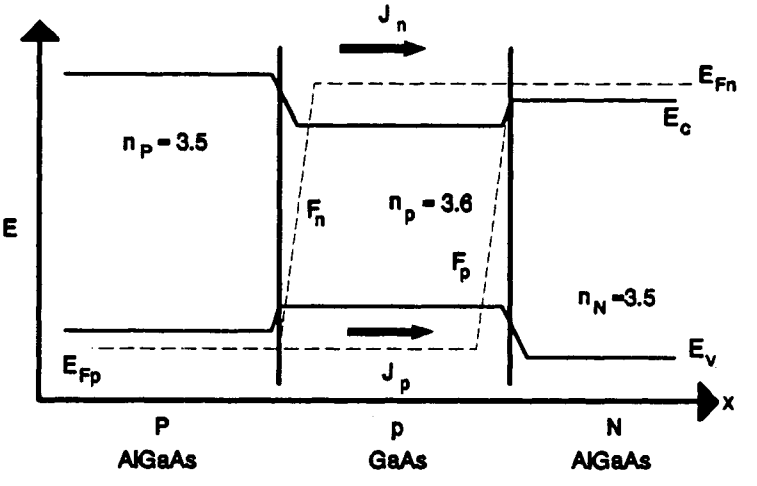

Figure 2.3 PpN Laser Diode Energy Band Diagram Under Forward Bias F_n -Electron Quasi-Fermi Level. F_p - Hole Quasi-Fermi Level. E_{FP} - Equilibrium Fermi Level p type AlGaAs. E_{FN} - Equilibrium Fermi Level n type AlGaAs. η_P - P AlGaAs Index of Refraction. η_p - p GaAs Index of Refraction. η_N - N AlGaAs Index of Refraction.

A laser diode that is constructed with a double heterojunction structure is a device in which three semiconductor materials of varying band gap are grown on top of each other resulting in an energy band diagram, under forward bias, as shown in Fig. 2.3. The term heterojunction, as defined by Streetman [11], refers to a junction that is formed between two lattice matched semiconductors with different band gaps. The double heterojunction refers to the fact that there are actually two heterojunctions that make up the device. In Fig. 2.3 these heterojunctions exist between the Pp and pN semiconductor regions.

A PpN device is illustrated in Fig. 2.3 because the PpN structure is a common type of double heterojunction laser diode [12]. The same energy band structure under equilibrium conditions is shown in Fig. 2.2. It should be noted that the capital letters in the PpN designation denote the wider band gap material. The energy band structure illustrated in Fig. 2.3 can be realized with a p type AlGaAs wide band gap semiconductor grown beside a p type narrow band gap GaAs semiconductor which is in turn grown beside an n type wide band gap AlGaAs semiconductor. Fig. 2.3 also illustrates typical values for the refractive indices of the different semiconductor materials present in the device structure. The carrier confinement feature of the double heterojunction device is also illustrated in Fig. 2.3. From the illustration it can be seen that there exists an energy barrier at the Pp heterojunction that confines the electrons to the active p region of the device. The difference in the energy bands of the p type AlGaAs and the p type GaAs prevents a significant reduction of the barrier height under forward bias thus preventing electron flow from the p to P region. An analogous situation for holes occurs at the pN heterojunction. The presence of the heterojunction energy band mismatch between the p type GaAs and the N type AlGaAs prevents a significant reduction in the valence band energy barrier. As a consequence, the holes are not allowed to flow from the p to N region and are thus confined in the active p region of the device structure.

The shape of the Quasi-Fermi levels in the device energy band diagram indicate

that the device depicted in Fig. 2.3 is not in equilibrium. Streetman [11] defines Quasi-Fermi levels as the steady state analogues of the equilibrium Fermi level. When excess carriers are present, the deviations of the Quasi-Fermi levels from the equilibrium Fermi level indicate how far the electron and hole populations are from their equilibrium values. The electron and hole current densities are proportional to the gradient of the Quasi-Fermi levels as per the following equations defined by Pierret [13].

$$J_p = \mu_p P \nabla F_p \tag{2.2}$$

$$J_n = \mu_n N \nabla F_n \tag{2.3}$$

As with an ordinary pn junction, the applied junction voltage V_j can be multiplied by the electronic charge and equated to the energy difference between the Quasi-Fermi levels as per Streetman [11].

$$qV_j = E_g + (F_n - E_c) + (E_v - F_p) \tag{2.4}$$

In the derivation of the expressions for the laser diode equivalent circuit electrical current components and the laser diode junction voltage components it is useful to remove the added complexity of the spatial dependence of the conduction band electron density and the valence band hole density by defining total spatial averages for these values in the active region.

$$N = N_o + n \tag{2.5}$$

$$P = P_o + p \tag{2.6}$$

The total spatial average value for the conduction band electron density is N and it is equal to the sum of the equilibrium conduction band electron density N_o and the excess conduction band electron density n. An analogous expression for the total average value of the valence band hole density is presented in equation (2.6). Throughout the rest of this work it is assumed that the spatial variations of the electron and hole densities are small and therefore these quantities can be represented by constant average values, consequently neither N, N_o, n, P, P_o or p are a function of the spatial variable x as per Tucker [14]. For the sake of simplicity, the assumption is made that the active region band gap E_g is not a function of the electron density N.

For the most part, the equivalent circuit of Fig. 2.1 models the active region of the laser diode with the exception of the resistor R_s which models the resistance of the package terminal lead and the near-ohmic pP isotype heterojunction as per Tucker [14]. The depletion capacitance has not been modelled since a laser is normally operated under forward bias where diffusion capacitance is dominant. Under gain switching conditions the device is routinely biased very near to the threshold level and it has been shown by Tucker [14] that under such conditions of relatively high forward bias current, the effect of the depletion capacitance is small. The laser diode equivalent circuit model proposed by Elkadi [15] does not model the depletion capacitance effect.

2.2 Derivation of the Laser Diode Junction Voltage Components

The derivation of expressions for the laser diode equivalent circuit junction voltage components begins with the fundamental definition of the total average conduction band electron density N and the total average valence band hole density P. Both N And P can be expressed in terms of the Fermi Dirac integral, the conduction and valence band energy levels E_c and E_v, the Quasi-Fermi levels for electrons and holes F_n and F_p, the conduction and valence band densities of states N_c and N_v, Boltzmann's constant k and the temperature in Kelvin T.

$$N = N_c \mathcal{F}_{\frac{1}{2}}\left[\frac{F_n - E_c}{kT}\right] \tag{2.7}$$

$$P = N_v \mathcal{F}_{\frac{1}{2}}\left[\frac{E_v - F_p}{kT}\right] \tag{2.8}$$

Tucker [14] approximates the Fermi-Dirac integrals using a power series which, if truncated after the first two terms, yield

$$\frac{F_n - E_c}{kT} = \ln\left(\frac{N}{N_c}\right) + \alpha_1 N \tag{2.9}$$

$$\frac{E_v - F_p}{kT} = \ln\left(\frac{P}{N_v}\right) + \alpha_2 P \qquad (2.10)$$

The constants α_1 and α_2 can be selected such that a close approximation to the Fermi Dirac integral can be obtained over a wide range of electron and hole densities as per Tucker [14].

The active p region has a low concentration of donor atoms which, for the purposes of Tucker's derivations, can be neglected. The ionized acceptor concentration N_A^- can be expressed as

$$N_A^- = \frac{N_A}{1 + 2e^{\frac{E_A - F_p}{kT}}} \qquad (2.11)$$

E_A represents the energy level of the acceptor atoms and N_A represents the concentration of the acceptors. The ratio of filled to unfilled acceptor sights has a form that is similar to the Fermi function as outlined in Pierret [13]. The factor of 2 in front of the exponential reflects the fact that the statistics that describe the filling of energy band levels differs from the statistics of filling levels within the energy band gap. The factor of 2 is called the acceptor-site degeneracy factor.

For zinc and germanium impurities, the acceptor energy level is about equal to the valence band energy level E_v and if this approximation is made and (2.10) is substituted into (2.11) then we get

$$\frac{N_A^-}{N_A} = \frac{1}{1 + 2e^{\frac{E_v - F_p}{kT}}} = \frac{1}{1 + 2\left(\frac{P}{N_v}\right)e^{a_2 P}} \qquad (2.12)$$

Tucker [14] demonstrates that equation (2.13) is an accurate approximation of (2.12) for a wide range of hole concentrations. The coefficient ξ is chosen to provide a good match between equations (2.12) and (2.13).

$$\frac{N_A^-}{N_A} = 1 - \xi\frac{P}{N_v} \qquad (2.13)$$

An equation can be written that describes the charge neutrality condition in the active region. For charge neutrality, the total hole concentration must be equal to the total electron concentration plus the concentration of ionized acceptor sites.

$$P = N + N_A^- \qquad (2.14)$$

Substituting (2.13) into the charge neutrality equation of (2.14) yields equation (2.15).

$$P = N + N_A - N_A\xi\frac{P}{N_v}$$

$$P\left(1 + \xi\frac{N_A}{N_v}\right) = N + N_A \qquad (2.15)$$

At thermal equilibrium equation (2.15) becomes equation (2.16) where the total electron and hole densities are replaced with their equilibrium components.

$$P_o\left(1 + \xi\frac{N_A}{N_v}\right) = N_o + N_A \qquad \textbf{(2.16)}$$

Since equation (2.15) is in terms of total electron and hole densities and equation (2.16) is in terms of equilibrium electron and hole densities, we can subtract (2.16) from (2.15) to obtain an expression in terms of the excess electron and hole densities as per equation (2.17)

$$p\left(1 + \xi\frac{N_A}{N_v}\right) = n \qquad \textbf{(2.17)}$$

Substituting equations (2.17), (2.16), (2.9) and (2.10) into equation (2.4) facilitates in the derivation of the laser diode junction voltage expression that consists of three components suitable for implementation in PSPICE specifically the resistive component R_1 and the two diode components D_1 and D_2. In equation (2.4) we defined the laser diode junction voltage V_j multiplied by the electronic charge in terms of the separation between the Quasi-Fermi levels. Equation (2.4) is equivalent to equation (2.18) below multiplied by the electronic charge q.

$$V_j = V_1 + V_2 + V_3 \tag{2.18}$$

Where

$$V_1 = V_{th}\left(\alpha_1 + \frac{\alpha_2}{\left(1 + \xi\frac{N_A}{N_v}\right)}\right)n \tag{2.19}$$

$$V_2 = V_{th}\ln\left(1 + \frac{n}{N_o}\right) \tag{2.20}$$

$$V_3 = V_{th}\ln\left[1 + \frac{n}{N_A + N_o}\right] \tag{2.21}$$

In the above three equations V_{th} represents the thermal voltage constant kT/q. Equations (2.19), (2.20) and (2.21) are ideal for implementation in PSPICE since they represent the mathematical definitions of the current voltage characteristics of a resistor and two diodes respectively. We can invert equations (2.19), (2.20) and (2.21) and equate each of the three to I_{spon}.

$$I_{spon} = \frac{V_1}{R_1} \tag{2.22}$$

$$I_{spon} = I_{01}\left(e^{\frac{V_2}{V_{th}}} - 1\right) \tag{2.23}$$

$$I_{spon} = I_{02}\left(e^{\frac{V_3}{V_{th}}} - 1\right) \tag{2.24}$$

Where I_{01} and I_{02} are the saturation current constants for the diode components D_1 and D_2 and are defined as follows.

$$I_{01} = \frac{q\Psi N_o}{\tau_{ns}} \tag{2.25}$$

$$I_{02} = \frac{q\Psi(N_A + N_o)}{\tau_{ns}} \tag{2.26}$$

The resistance component R_1 is defined in (2.27) such that the Ohm's law relationship of equation (2.22) holds true.

$$R_1 = \frac{\left(\alpha_1 + \frac{\alpha_2}{\left(1 + \xi\frac{N_A}{N_v}\right)}\right)N_o V_{th}}{I_{01}} \tag{2.27}$$

Now that the laser diode junction voltage expressions are established, it is clear that the current drawn by these components is equivalent to the excess spontaneous recombination current I_{spon} that is proportional to n.

2.3 Derivation of the Laser Diode Equivalent Circuit Electrical Current Components

The total device current, excluding the component for stimulated emission, is defined in this work as I_e and is established in equation (2.28). A time dependent differential term has been added to account for the charge storage current component in the active region. A physical justification with accompanying derivation of the time rate of change term is provided in appendix A.

$$I_e = q\Psi\left(\frac{n}{\tau_{ns}} + \frac{dn}{dt}\right) \qquad (2.28)$$

The variables A and d in equation (2.28) are the same as those defined in Fig. 1.1 of chapter one and represent the area and the width of the laser diode active region respectively. An equation in terms of I_{spon} can be derived by substituting in I_{spon} where appropriate.

$$I_e = q\Psi\left[\frac{n}{\tau_{ns}} + \frac{dn}{dt}\right]$$
$$= \frac{qn\Psi}{\tau_{ns}} + q\Psi\frac{dn}{dt}$$

$$I = I_{spon} + \tau_{ns}\frac{dI_{spon}}{dt} \qquad (2.29)$$

It should be noted at this stage that the terms that make up equation (2.29) represent the electrical current components of the equivalent circuit model, excluding the stimulated emission component, and are all written in terms of I_{spon}. This particular way of writing the current component in terms of I_{spon} is intentional since the equations that represent the laser diode junction voltage components can also be written in terms of the quantity I_{spon}. In fact the stimulated emission current component which is defined in section 2.4 is also written in terms of the quantity I_{spon}. Writing the junction voltage components in terms of the same quantity that we write the electrical current component defines the current voltage characteristic of the laser diode.

This concludes the derivation of the electrical current components I_e, excluding the stimulated emission component which will be dealt with in section 2.4.

2.4 Derivation of the Optical Components of the Laser Diode Equivalent Circuit Model

In this section the optical components located on the right half of the laser diode

equivalent circuit model of Fig. 2.1 are derived, specifically the capacitive component C_{ph}, the resistive component R_{ph}, the spontaneous emission coupling current source βI_{spon} and the stimulated emission current component, which is also the stimulated emission photon source I_{stim}.

The derivation of the electrical current voltage characteristics of the laser diode that was undertaken in the last two sections was based on Tucker's derivation and provide the mathematical framework for modelling the junction voltage across the laser diode in terms of the current injected into the laser diode. In this section the optical half of the laser diode equivalent circuit model will be derived and in order to derive the mathematical form of the optical component expressions it is necessary to refer back to the laser diode rate equations introduced in chapter one. The two halves of the circuit are, in effect, a combination of the mathematical framework of Tucker and Jones. In the interest of completeness, the laser diode rate equations are restated below.

$$I = I_{spon} + \tau_{ns}\frac{dI_{spon}}{dt} + \tau_{ns}g_o I_{spon}\phi \qquad (2.30)$$

$$q\Psi\frac{d\phi}{dt} = \tau_{ns}g_o I_{spon}\phi - \frac{q\Psi\phi}{\tau_{ph}} + \beta I_{spon} \qquad (2.31)$$

It should be noted that Ψ in the above equations represents the volume of the active region $d \times A$, g_o represents the optical gain constant for the laser diode and τ_{ph} represents the photon lifetime.

It is desirable to replace the photon density ϕ with a normalized version hereafter referred to as ϕ' which enables manageable numerical values to be obtained for elements in the circuit model as per Tucker [6]. The constant ϕ_n in equation (2.32) is the photon density scaling parameter.

$$\phi' = \frac{\phi}{\phi_n} \tag{2.32}$$

Once the rate equations have been manipulated into the form shown in equations (2.30) and (2.31), the different terms can be associated with various elements in the optical half of the laser diode equivalent circuit model.

The coupling between the electron and photon densities in both of the rate equations is represented by the nonlinear current source term I_{stim}.

$$I_{stim} = \tau_{ns} g_o I_{spon} \phi \tag{2.33}$$

The resistance component R_{ph} models the photon losses in the laser cavity. R_{ph} is defined as shown in equation (2.34).

$$R_{ph} = \frac{\tau_{ph}}{q \Psi \phi_n} \tag{2.34}$$

The current through R_{ph} is derived by noting that the voltage representing the scaled photon density in the circuit ϕ' is also the voltage that is dropped across the resistance R_{ph}. We can obtain the current through this resistor by the Ohm's law relationship.

$$\frac{\frac{\phi'}{\tau_{ph}}}{q\Psi\phi_n} = \frac{\phi q\Psi\phi_n}{\phi_n\tau_{ph}} = \frac{\phi q\Psi}{\tau_{ph}} \tag{2.35}$$

Note that the current through the resistor, defined in equation (2.35), is equivalent to the photon cavity loss term in the photon density rate equation of (2.31).

The C_{ph} term models the time derivative of the photon density term in equation (2.31). The current through the capacitor C_{ph} can be written as

$$C_{ph}\frac{d\phi'}{dt} = q\Psi\phi_n\frac{d\left(\frac{\phi}{\phi_n}\right)}{dt} = \frac{q\Psi\phi_n}{\phi_n}\frac{d\phi}{dt} = q\Psi\frac{d\phi}{dt} \tag{2.36}$$

Note that the current through the capacitor C_{ph} is equivalent to the time rate of change of the photon density term in equation (2.31).

The βI_{spon} current source in the laser diode equivalent circuit model accounts for the increase in the photon density due to the photons that couple into the lasing mode from spontaneous emission. The constant β represents the spontaneous emission coupling coefficient. With all the elements in the laser diode equivalent circuit defined it is now possible to discuss the implementation of the equivalent circuit model in PSPICE.

2.5 Implementation of the Laser Diode Equivalent Circuit Model in PSPICE

Although the derivations of the mathematical expressions for the various

components of the laser diode equivalent circuit model are, for the most part, straightforward, some of the details of the PSPICE implementation are not obvious. In this section the PSPICE implementation details are explained.

The laser diode equivalent circuit model of Fig. 2.1 is repeated below with the simulation nodes included in the illustration.

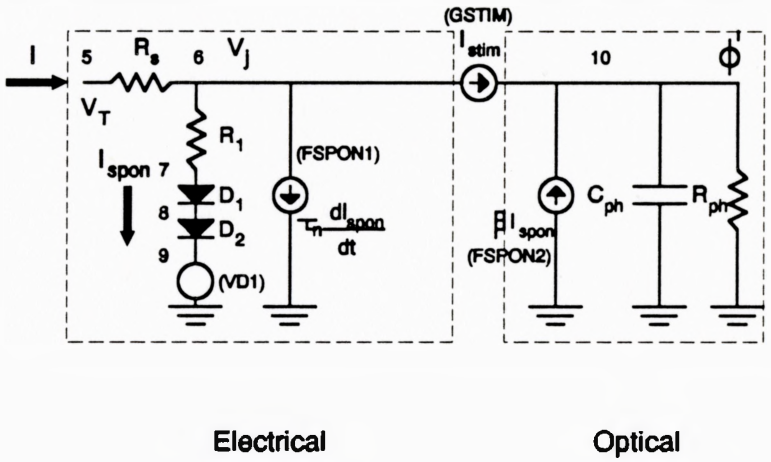

Figure 2.4 Laser Diode Equivalent Circuit Model (Identical to figure 2.1 with the addition of simulation circuit nodes and PSPICE circuit definition file source names)

One of the details in the PSPICE implementation that is not obvious is the

implementation of the nonlinear current source I_{stim} that accounts for the stimulated emission current component and the photon contribution from stimulated emission. The stimulated emission term is proportional to the excess conduction band electron density multiplied by the photon density in the lasing cavity. A scaled version of the photon density ϕ' is obtained directly from node (10) in the equivalent circuit model of Fig. 2.4. The conduction band electron density is more difficult to obtain. A zero voltage DC source V_{D1} is placed between node (9) and ground. In PSPICE the zero voltage DC source functions as a current meter. The subcircuit shown in Fig. 2.5 is implemented with a current controlled current source placed in series with a resistor of value τ_{ns}. By Ohm's law the voltage at node (14) will be

$$V_{(14)} = I_{spon}\tau_{ns} = \tau_{ns}\left[\frac{q\Psi n}{\tau_{ns}}\right] = q\Psi n \qquad (2.37)$$

The voltage at node (14) is equal to the excess conduction band electron density scaled by the electronic charge q and the active region volume Ψ. The voltage at node (14) is used in a PSPICE polynomial statement as one of the products that make up the stimulated emission current source I_{stim}.

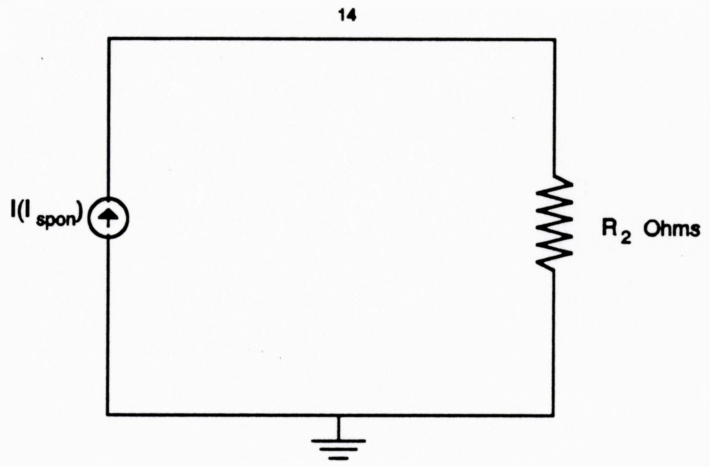

Figure 2.5 Stimulated Emission Subcircuit $R_2=\tau_{ns}$ Ohms This subcircuit is used to multiply out τ_{ns} from the I_{spon} current. $I(I_{spon})$ is a current controlled current source that reproduces the current I_{spon} from the laser diode equivalent circuit model. The voltage at node (14) is proportional to the excess conduction band electron density and is not multiplied by the inverse of the spontaneous emission lifetime constant τ_{ns}.

The τ_{ns} $(dI_{spon})/(dt)$ current source is implemented using the subcircuit of Fig. 2.6. A current controlled voltage source is placed in series with a zero volt DC voltage source and a capacitor of τ_{ns} Farads. The DC voltage source V_{D2} functions as a current meter. The current through the capacitor is proportional to the time rate of change of the voltage across the capacitor multiplied by the capacitance.

$$I_g = C_1 \frac{dV}{dt} \tag{2.38}$$

The current controlled voltage source is configured to output a voltage equivalent to the current component I_{spon} from the laser diode equivalent circuit model. The current through the voltage source V_{D2} can be written as per equation (2.38) as

$$I_g = \tau_{ns} \frac{dI_{spon}}{dt} \tag{2.39}$$

The current of equation (2.39) that passes through V_{D2} is used to control the $\tau_{ns}(dI_{spon})/(dt)$ current source in the laser diode equivalent circuit model.

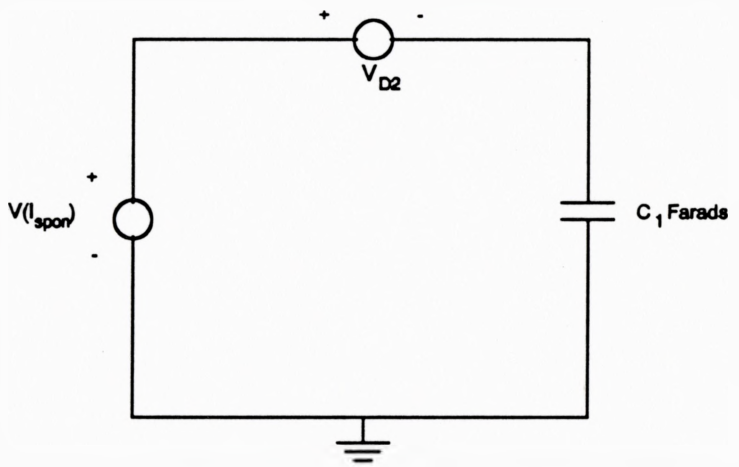

Figure 2.6 $\tau_{ns}(dI_{spon})/(dt)$ Current Source Subcircuit $C_1 = \tau_{ns}$ Farads. The subcircuit source outputs a voltage equivalent to I_{spon} from the laser diode equivalent circuit model. The current that passes through the capacitor C and the current meter voltage source V_{D2} is equivalent to $\tau_{ns}(dI_{spon})/(dt)$ and is used to implement the corresponding current source in the laser diode equivalent circuit model.

With the form and implementation of the laser diode equivalent circuit model established, it is now possible to proceed to the next chapter where the model is compared to the various analytical responses derived in chapter one.

Chapter 3: Circuit Model Verification and Gain Switching

In this chapter the laser diode equivalent circuit model simulations implemented in PSPICE are compared to the analytical solutions presented in chapter one for the DC, AC small signal and gain switched transient cases. At the end of the chapter, a basic gain switching experiment is described along with a comparison of the experimentally measured pulse width to the simulated gain switched pulse width. A measurement of the terminal voltage of the laser diode during gain switching is presented and compared with a PSPICE simulation of the gain switching experiment electronics.

3.1 Model Verification

DC Excitation

For the DC excitation case, the light emitted from the laser is assumed to be zero until the threshold current is reached. Beyond threshold current, the output photon density is related to the input DC current that is in excess of threshold by the following

equation from chapter one repeated below for convenience.

$$\phi_{dc} = \frac{1}{g_o n_{th}}\left[\frac{I - I_{th}}{q\Psi}\right] \tag{3.1}$$

Fig. 3.1 is a comparison of the analytically calculated DC solution with the solution as predicted by the laser diode equivalent circuit simulation implemented in PSPICE. The photon density is related to the optical output power by equation (3.2) where h is Plank's constant, υ is the frequency of the light, c is the speed of light, η is the index of refraction of the active region, w is the width of the active region and d is the thickness. For a pictorial view of the dimensions of the active region, the reader is referred to Fig. 1.1.

$$P_o = h\upsilon\frac{c}{\eta}\phi wd \tag{3.2}$$

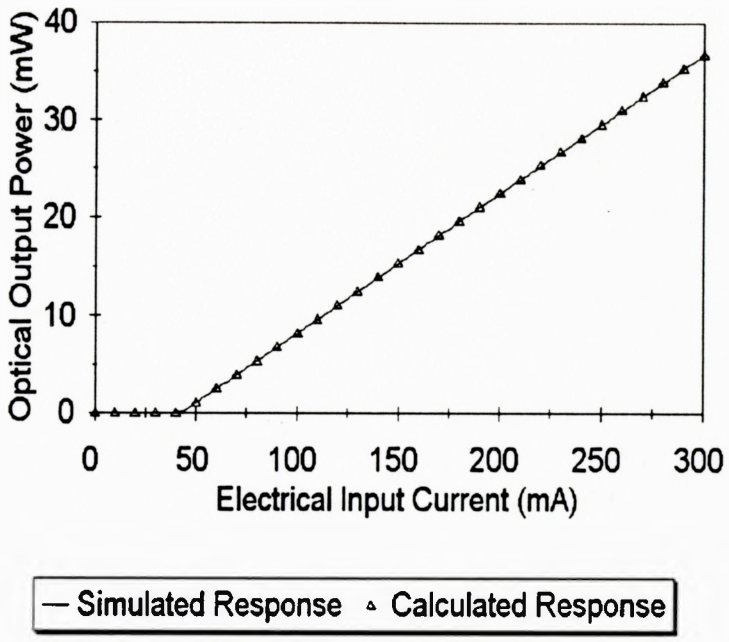

Figure 3.1 DC Optical Output Power Versus Input Current Input Current I (mA). Comparison of PSPICE equivalent circuit model simulated and analytically calculated response. Parameter values used in the simulation and calculation are:

τ_{sp}	Spontaneous Recombination Lifetime	4.8×10^{-10} s
τ_p	Photon Lifetime	1.0×10^{-12} s
β	Spontaneous Coupling Coefficient	2.0×10^{-4}
q	Electronic Charge	1.6×10^{-19} Coulombs
V_a	Active Region Volume	4.125×10^{-16} m^3
I_{th}	Laser Threshold Current	42.0×10^{-3} Amps
η	Index of Refraction of Active Region	3.60
υ	Light Frequency	375×10^{12} Hz
w×d	Area of the Active Region Perpendicular to Light	9.1×10^{-13} m^2
g_o	Gain Constant	3.2×10^{-12} m^3/s

The parameters of the circuit elements that comprise the junction voltage of the laser diode equivalent circuit were defined as $I_{01} = 2.059\times10^{-14}$ Amps, $I_{02} = 2.059\times10^{-14}$ Amps and $R_e = 1.5498$ Ohms. These parameter values are consistent with an impurity

acceptor concentration in the active region of $N_A = 0.0\ m^{-3}$, an equilibrium electron concentration of $N_o = 1.5\times10^{11}\ m^{-3}$, a thermal voltage of $V_{th} = 25.9$ mV and the α_1 parameter as defined in chapter two is $\alpha_1 = 8.226\times10^{-24}\ m^3$.

As can be seen from Fig. 3.1, the DC solution of the rate equations, as predicted by the laser diode equivalent circuit simulation, is in good agreement with the analytically calculated DC solution. The high degree of agreement between the analytically calculated result of the DC solution and the laser diode equivalent circuit model simulation is to be expected since in essence the same equations are being solved analytically and numerically. The fact that the two curves agree so well confirms that the assumptions made in deriving the analytical solution of the rate equations for the DC case are in fact valid.

AC Small Signal Excitation

The principal equation governing the normalized AC small signal excitation light output was presented in chapter one and is repeated below for convenience.

$$M(\omega_m) = \frac{1}{\left(1 - \frac{\omega_m^2}{\omega_o^2}\right) + j\frac{2\alpha\omega_m}{\omega_o^2}} \qquad (3.3)$$

Fig. 3.2 is a comparison of the analytically calculated AC small signal solution

with the simulated solution of the laser diode equivalent circuit model implemented in PSPICE.

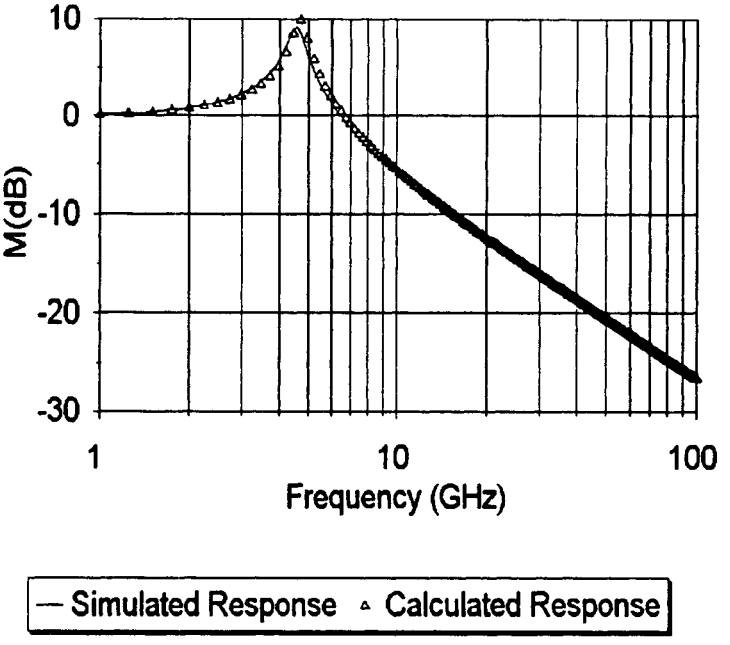

Figure 3.2 Frequency Response of M(dB) M is defined in equation (1.27) and is in units of (dB). Comparison of PSPICE simulation response with the analytically calculated response. Laser diode parameters are the same as in Fig. 3.1 with the addition of a current modulation index m_i - 0.0167. I_b = 60 mA.

Again it can be seen that there is a very good agreement between the analytically calculated AC solution to the rate equations and the laser diode equivalent circuit model simulation of the AC response. The reasons for the excellent agreement between the analytically calculated AC response and the simulated AC response are the same as those mentioned above for the DC case.

Gain Switching

The laser equivalent circuit model discussed in chapter two that models the coupled nonlinear rate equations predicts a gain switched response when the laser is biased near threshold and subject to current pulses of 80 ps duration with amplitudes several times the threshold current. In chapter one, an analytical solution to the rate equations for gain switching was presented. The equations that were developed that described the gain switched pulse width and time delay can be used to verify the accuracy of the laser diode equivalent circuit model. The equations describing these important pulse characteristics from chapter one are repeated below for reference.

Pulse response characteristics were calculated analytically and compared with the simulated response from the laser diode equivalent circuit model as a function of various applied current pulse amplitudes with a pulse width fixed at 80 ps.

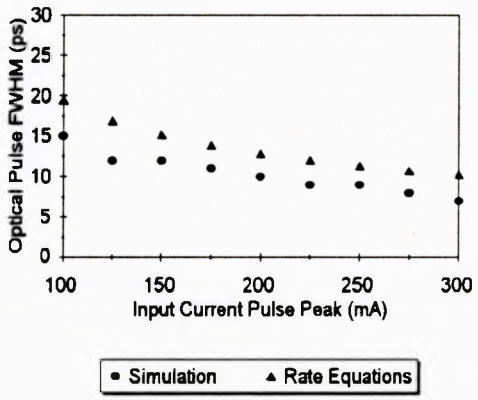

Figure 3.3 Gain Switched FWHM Pulse Width Comparison A comparison between the analytically calculated output optical pulse width and the PSPICE laser diode equivalent circuit model simulated optical pulse width.

The analytical equation that governs the pulse width was derived in chapter one and is repeated below.

$$\Delta t = \sqrt{\frac{8\ln 2}{g_o u}} \tag{3.4}$$

As can be seen from Figure 3.3, the theoretically calculated gain switched pulse width is in good agreement with the simulated pulse width with a difference of approximately 3 ps. The reason there is a difference between the simulated pulse width and the analytically calculated pulse width goes back to the assumptions that are made in deriving the analytical formula of (3.4) for the pulse width. The derivation of the analytical formulas for the gain switched response assumes that the excess conduction band electron density is a linear function of time. The laser diode equivalent circuit model simulation solves the rate equations numerically and thus accounts for the nonlinearity of the excess conduction band electron density.

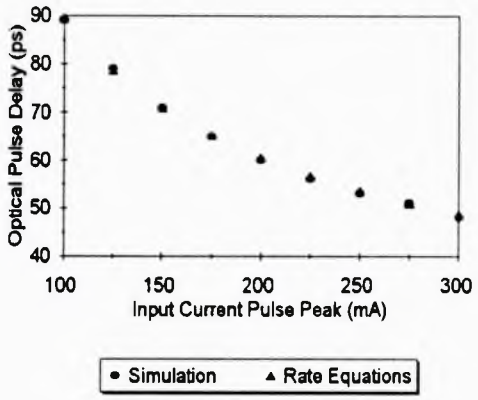

Figure 3.4 Gain Switched Optical Pulse Delay Comparison A comparison of the analytically calculated and the simulated time delay between the electrical current pulse and the appearance of the gain switched optical pulse.

There is excellent agreement between the equivalent circuit model simulation and the analytical calculation of the time delay between the initiation of the input current pulse and the appearance of the output optical pulse as per Fig. 3.4.

As can be seen from the above two figures, the trends predicted by both models are the same and in all cases the laser diode equivalent circuit model is in good agreement with the analytically derived pulse characteristics.

3.2 Gain Switching Experiments

The experiments that were carried out to study the gain switching characteristics of the SHARP laser diodes used in this work were done with a conventional step recovery diode pulse generator, specifically the Hewlett Packard Series 3300X. The

characteristics of step recovery diodes will be discussed fully in chapter four however it should be mentioned at this stage that the step recovery diode, or SRD as it is commonly referred to, is a semiconductor device that can be used to build a pulse train generator when combined with other circuit elements. The typical output pulse train from the SRD pulse generator circuit consists of pulses of less than 100 ps FWHM and approximately 300 mA peak current amplitudes into 50 Ohms. SRD pulse generators are usually driven with an oscillator tuned to the frequency to which the pulse generator is tuned. Depending on the power available from the oscillator, an amplifier may be required between the oscillator and the SRD pulse generator. The apparatus used in these gain switching experiments is shown below.

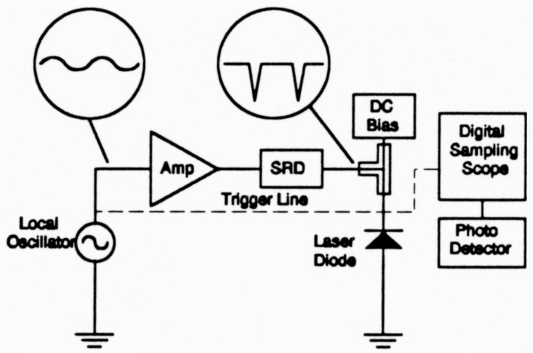

Figure 3.5 Apparatus For Conventional Gain Switched Laser Diode Pulse Measurements In this experiment the laser diode was a SHARP LT015MF0 device. The amplifier was a Mini Circuits ZHL-1A 16 dB unit with a bandwidth of DC to 500 MHz. SRD pulse generator was a Hewlett Packard 33004 device capable of generating $<$ 100 ps pulses of 300 mA amplitude into 50 Ohms. The photodetector was an Antel AR-S2 detector with a pulse response of $<$ 65 ps. The digital sampling oscilloscope had a bandwidth of 20 GHz.

A tuned 500 MHz SRD pulse generator was used exclusively in the gain switching experiments reported in this chapter. In order to collimate the light from the device, a collimating lens was placed between the laser diode source and the photo-detector. In practice the optimum positioning of the collimating lens is achieved by sliding it along a rail that is parallel to the direction of light propagation until it is observed that the light is collimated. The position of the detector is then adjusted using an xyz translation stage until the maximum obtainable detector current swing is observed. When these adjustments are completed, the system is ready for gain switching measurements.

The gain switching experiments were carried out with different photo-detectors of varying speeds, the fastest of which had a pulse response of 65 ps. The optical gain switched pulse that was observed is shown below in Figure 3.6.

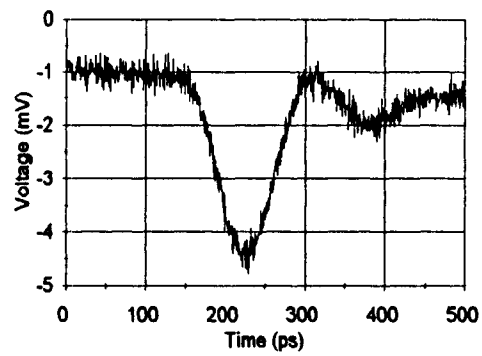

Figure 3.6 Gain Switched Pulse Measurement Laser diode bias current was approximately $0.75I_{th}$. The measurement was taken with a 65 ps FWHM photodetector.

This gain switched pulse from a SHARP LT015MF0 laser diode shown above is approximately 77 ps long. When the 65 ps rise time of the photodetector and the 25 ps rise time of the 20 GHz digital sampling oscilloscope are accounted for, the gain switched pulse width is estimated to be approximately 30 ps. The analytical formula for this deconvolution is presented in appendix B.

3.3 Laser Diode Terminal Voltage Measurement and Simulation

The purpose for implementing a laser diode equivalent circuit model in this work was to be able to qualitatively predict the light output from the device and to qualitatively predict the electrical interaction between the laser diode and the other elements of the driver circuit. Measurements of the time response of the laser diode terminal voltage were made during the gain switching experiments. The goal was to compare the measured electrical response of the laser diode terminal voltage during gain switching and the simulated terminal voltage predicted by the PSPICE laser diode equivalent circuit model. A simulation circuit of the experimental apparatus was implemented in PSPICE which included an equivalent circuit model for the laser diode, an equivalent circuit model for the SRD, two DC blocking capacitors and a DC bias inductor. A resistor is also placed in series with the DC blocking capacitor. In addition there is a DC current bias placed on the semiconductor laser diode as well as a sinusoidal power supply which drives the SRD. In practice, the DC bias was set to between $0.75I_{th}$ and $0.9I_{th}$ of the

laser diode under test. The sinusoidal source was set to a frequency of 500 MHz and a peak amplitude of approximately 5 volts.

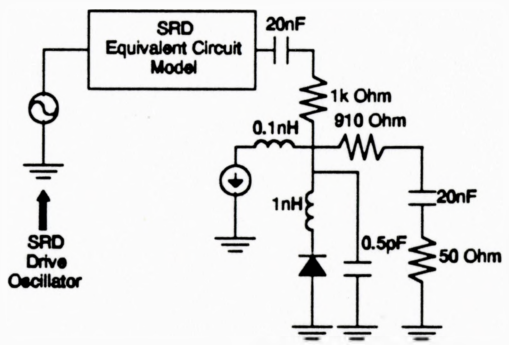

Figure 3.7 System Diagram of Gain Switching Experiment Electronics. The above diagram is a simplified representation of the electronic components present in the gain switching experiment and the PSPICE circuit model.

Fig. 3.7 represents a system level diagram of the gain switching experiment electronics. It should be noted that the in practice it was necessary to place an amplifier between the 500 MHz oscillator and the SRD. Since the voltage level of the sinusoidal signal source can be set to any arbitrary value in PSPICE, the amplifier is not included in the simulation of the gain switching electronics.

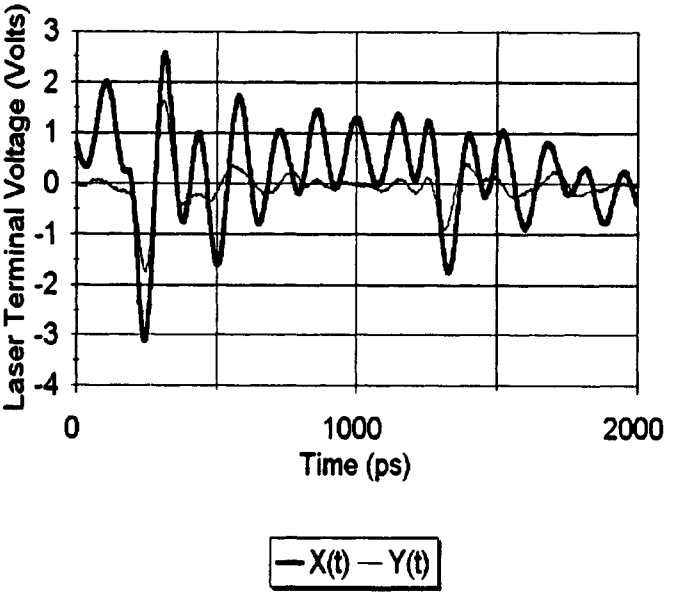

Figure 3.8 Measurement of the Laser Diode Terminal Voltage X(t) - Deconvolved Terminal Voltage Measurement. Y(t) - Terminal Voltage Measurement Before Deconvolution

Fig. 3.8 represents the measured terminal voltage characteristic of the SHARP LT022MF0 semiconductor laser diode during gain switching. The actual raw data measured from a Hewlett Packard 54120A 20 GHz Digital Sampling Oscilloscope is shown as curve Y(t) in Fig. 3.8. A frequency response measurement of H(f) of the laser diode in its encasement module was made on a Hewlett Packard 8510B Network Analyzer between the electrical input of the laser diode encasement module and the electrical output.

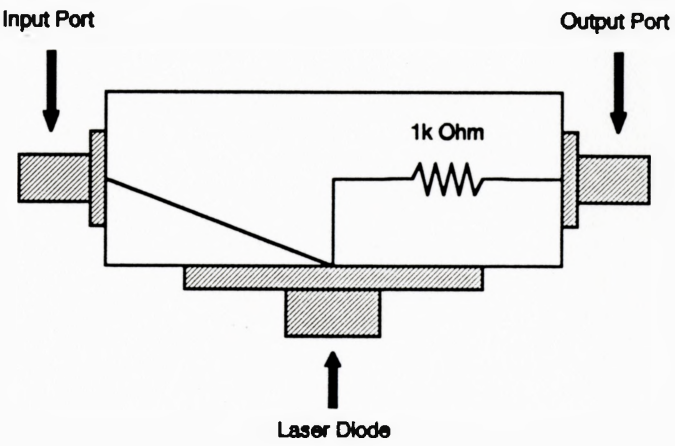

Figure 3.9 Schematic of Laser Diode and Encasement. The input and output ports are labelled.

Fig. 3.9 illustrates a schematic of the laser diode and the encasement module. The anode of the laser diode was tied to ground and the cathode was tied to the input port to which the SRD output was connected. A 910 Ohm resistor was placed in series with the output port to prevent excessive loading of the current pulse from SRD due to the scope probe.

The voltage X(t) on the terminals of the laser diode under gain switching conditions appears on the input port to the laser diode module. The output Y(t) that is measured on the oscilloscope is the input voltage convolved in time with the impulse

response of the laser diode and its encasement module. The actual input X(t) can be retrieved from the measured data by deconvolving the impulse response of the laser diode and the encasement module from the measured response Y(t). Since deconvolution in the time domain corresponds to division in the frequency domain, X(f) can be obtained by performing the frequency division as described by equation (3.5).

$$X(f) = \frac{Y(f)}{H(f)} \tag{3.5}$$

X(f) can then be Fourier transformed to obtain X(t) which is the terminal voltage of the semiconductor laser diode. From Fig. 3.8, it is observed that the voltage X(t) on the laser diode terminals consists of a damped oscillation in response to the SRD pulse that extends from approximately 300 ps to 1250 ps. The frequency of this oscillation is approximately 7 GHz. There is no DC shift observed in the measured data because there was a DC blocking capacitor between the measurement terminal and the scope probe.

In the PSPICE simulation of the gain switching experiment electronics, we see the presence of a DC shift which is to be expected for a semiconductor laser diode under DC forward bias. The PSPICE gain switching circuit simulation predicts a damped oscillation as shown in the measurement however it does not predict the secondary spike of increased amplitude at approximately 1350 ps. By choosing a value of 0.5 pF and 1.0 nH for the laser diode parasitics, as shown in Fig. 3.7, the PSPICE simulation predicts a damped resonance frequency of approximately 7.1 GHz, a value which is consistent with the measurements.

PSPICE simulations of the gain switching experiment electronics is shown in Fig. 3.10 where both the optical output and the terminal voltage characteristic of the laser diode are shown.

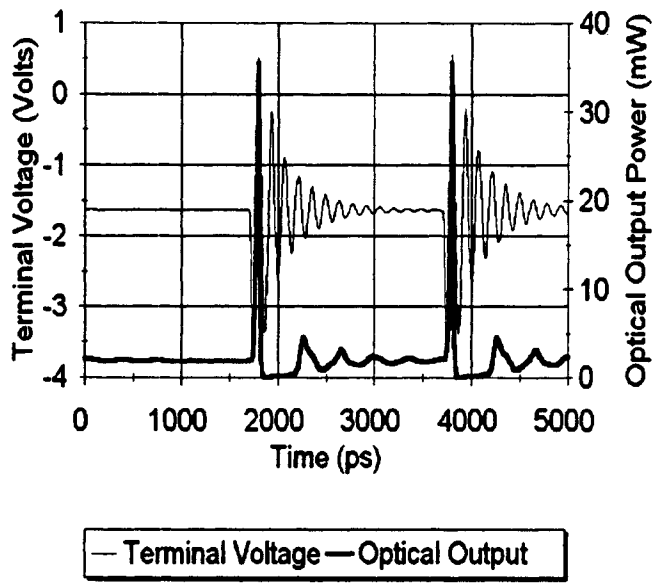

Figure 3.10 PSPICE Simulation Results of Gain Switching Experiment
The graph illustrates the simulation of the laser diode terminal voltage characteristics as well as the optical power output.

The reader should note that the measured value of the laser diode terminal voltage was taken from the cathode of the device with the anode grounded. With this configuration, a negative voltage measurement at the anode is to be expected.

There is relatively good agreement between the measured gain switched pulse width estimation and the simulated gain switched pulse width both having approximately

30-35 ps wide FWHM. The FWHM pulse width is the most important specification of the gain switched pulses when used in electro-optic sampling applications. Since the physical parameters of the devices simulated are not precisely known, it cannot be stated with certainty that the agreement between the experimentally measured and simulated pulse widths is not coincidental. It can be said that a good qualitative agreement exists between the experimental data and the simulation of the gain switching experiment electronics with respect to the characteristics of the measured laser diode terminal voltage, and the width of the experimentally estimated optical gain switched pulse.

A quantitative agreement between the simulations and the measurements is not possible where exact values of the physical parameters are not available. Where possible, typical values of the physical parameters used were taken from the literature. Determining these parameters experimentally was beyond the scope of this work.

Chapter 4: Gain Switched Laser Driver Techniques

In order to develop a gain switching laser driver circuit for electro-optic sampling applications, it is necessary to investigate various electronic methods of producing suitably short current pulses. To gain switch a semiconductor laser diode, the electronic driver must be capable of producing current pulses with a FWHM that is on the order of 100 ps with amplitudes that are approximately five times the threshold current as per Paulus [3]. An additional specification that is imposed on the design of the laser driver circuit by the electro-optic sampling system constraints is that the laser driver must be capable of producing pulses with a variable repetition rate. The device of choice for producing short electrical current pulses to gain switch a laser diode has traditionally been the step recovery diode (SRD) pulse train generator. In a later section of the chapter, the theory behind the SRD pulse train generator circuit is discussed along with the description of a PSPICE simulation of the device. The PSPICE simulation results are compared to experimental measurements of the SRD pulse train generator response. It is shown that a fixed repetition rate gain switched laser driver can easily be constructed with a step recovery diode using the configuration that is standard in most gain switching experiments presented in the literature such as Paulus [3]. A novel technique, referred

to as mono-cycling, that allows the step recovery diode to be fired at variable repetition rates is described with experimental measurements. A novel technique, referred to as bias modulation optical pulse quenching, which involves turning the DC bias to the laser diode on and off electronically to switch the optical pulses from the laser diode on and off is described. A PSPICE simulation of this circuit is discussed along with the implementation of the circuit and measurements.

4.1 Tradeoffs in Electro-Optic Sampling System Pulsed Light Source Design

Electro-optic sampling systems require a light source that is capable of generating extremely short optical pulses. Established research electro-optic sampling systems use commercial lasers capable of generating pulses on the order of 0.1 ps. In going from a commercial laser to a semiconductor laser diode there are some trade offs. The principal advantages of using a semiconductor laser diode in an electro-optic sampling system are

a) **Economy** - Semiconductor laser diodes are inexpensive. A 15 mW infra red laser diode costs about one hundred and fifty dollars. When compared to the cost of commercial Q-switched lasers, the economical advantages of using a laser diode are obvious.

b) **Size** - Semiconductor laser diodes are extremely compact. This is an obvious advantage when designing a compact and portable electro-optic sampling system.

c) **Simplicity** - Laser diodes are simple to use and with micro-electronic driver circuitry, the integrated driver package can be made extremely compact.

The disadvantages of using a semiconductor laser diode in an electro-optic sampling system are

a) **Pulse Width** - A semiconductor laser diode will generate pulse widths on the order of 20 ps when gain switched. The minimum pulse width that you can generate from a laser diode is considerably wider then the pulse widths that are available from commercial lasers.

b) **Driver Circuitry** - Specialized driver circuitry must be developed in order to gain switch a laser diode at variable repetition rates.

Various techniques for gain switching a laser diode are presented in this chapter. The advantages and disadvantages for each type of driver are discussed. The three types of laser driver techniques that will be discussed are referred to as

1) The Conventional SRD Laser Driver Technique

2) The Mono-Cycle SRD Laser Driver Technique

3) The Bias Control SRD Pulse Quenching Laser Driver Technique

Before discussing the details of the driver techniques investigated, it is useful to briefly discuss the step recovery diode pulse train generator which is a principal component in all three of the methods investigated.

4.2 Step Recovery Diode Pulse Train Generators

A step recovery diode pulse train generator is a circuit that combines a step recovery diode with various passive elements. When subjected to sinusoidal excitation at the tuned frequency and of sufficient amplitude the 500 MHz tuned Hewlett Packard device responds with a train that consists of extremely narrow pulses, on the order of 100 ps FWHM and 300 mA peak amplitude, at a repetition rate that corresponds to the excitation frequency. A brief description of how the diode works is useful before attempting an explanation of the pulse generator circuit.

A pn junction diode will exhibit a finite switching time as per Streetman [11].

If a diode is connected in series with a resistor and a square signal generator of sufficient amplitude, as shown in Fig 4.1, the diode will conduct during the forward cycle of the waveform and it will conduct for a portion of the negative cycle. The current conducted during this portion of the negative cycle will be of approximately the same magnitude as the current conducted during the forward cycle of the waveform.

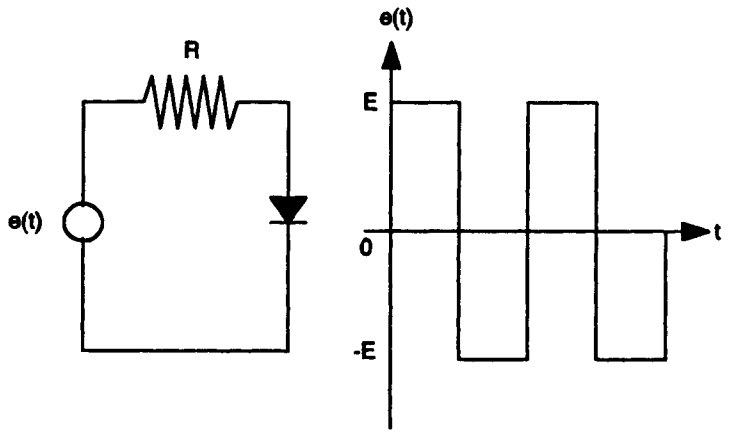

Figure 4.1 Semiconductor pn Junction Diode Experiment This experiment can be used to demonstrate the reverse recovery transient of a pn junction diode. e(t) is a signal generator of sufficient amplitude to forward bias the device. R is a current limiting resistor.

The reason that the device conducts during a portion of the negative cycle is because the pn junction stores charge while forward biased. The diode cannot turn off or develop a reverse voltage across it until there is a considerable change in the minority carrier density near the junction as per Streetman [11]. This is readily apparent from the following equation for the excess minority carrier density for holes on the n side of the junction.

$$\Delta p_n = p_n\left(e^{\frac{qV}{kT}} - 1\right) \tag{4.1}$$

Two important temporal parameters when discussing the turnoff time of the device are the storage time τ_s and the turn off time τ_o. The storage time of the device determines how long an appreciable amount of reverse current will conduct before diode begins to turn off. The turn off time determines how long it actually takes for the step recovery diode to turn off after the storage time has elapsed.

The voltage across the device must remain positive as long as Δp_n, the excess minority carrier density on the n side of the junction, is positive. A step recovery diode is designed to have a finite storage time τ_s, and to minimize the turn off time τ_o. These characteristics are not the same for switching diodes where any reverse conduction is undesirable. There are circuit applications where the required reverse recovery time is determined by the circuit as per Moll [16]. Reverse conduction is obtained in practice by having a finite carrier lifetime usually as long as can be obtained from the fabrication process as discussed by Moll [16].

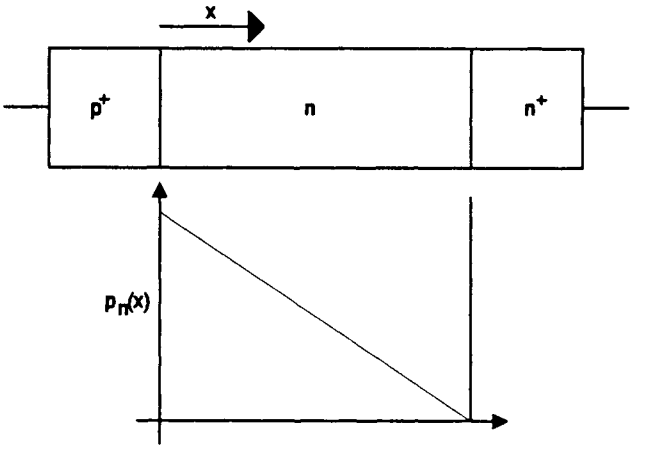

Figure 4.2 Physical Structure and Minority Carrier Density Distribution of a Step Recovery Diode. p^+ - Heavily Doped p Regio n. n^+ - Heavily Doped n Region. n - Doped Region. $p_n(x)$ - Minority Carrier Density Distribution (m^{-3})

The turn off time is minimized by designing the device such that the minority carriers are almost completely depleted when the minority carrier density at the junction reaches zero. This fact implies that there will be relatively few residual stored carriers that can flow back across the p^+n junction to slow up the establishment of a reverse voltage. Fig. 4.2 illustrates the physical structure of a step recovery diode and the distribution, as a function of the distance variable x, of the minority carrier density p_n (x). The origin of the distance is taken to be at the junction of the p^+n region.

A commercial SRD pulse generator consists of the SRD device and a circuit that is tuned to a specific frequency such as 100, 250 or 500 MHz. The device responds with

a pulse train at a repetition rate that corresponds to the excitation frequency to which it is tuned. The SRD pulse generator can be represented by the equivalent circuit shown in Fig. 4.3

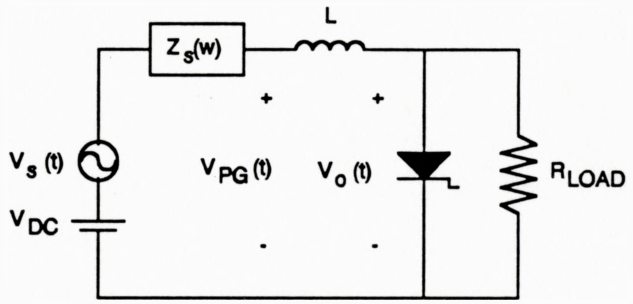

Figure 4.3 SRD Pulse Generator Equivalent Circuit $V_s(t)$ - Excitation Sinusoid. V_{DC} - Excitation DC offset Voltage. $Z_s(\omega)$ - Filter. L - Inductor Value (Henries). R_{LOAD} - Load Resistance (Ohms).

In order to develop analytical expressions that describe the operation of the circuit of Fig. 4.3, it is necessary to represent the circuit with two equivalent circuits that are each in effect during different time intervals of each period of the excitation sinusoid. Fig. 4.4 represents a graph of the simulation of the input excitation voltage and the

output voltage that appears across the step recovery diode and the load resistor.

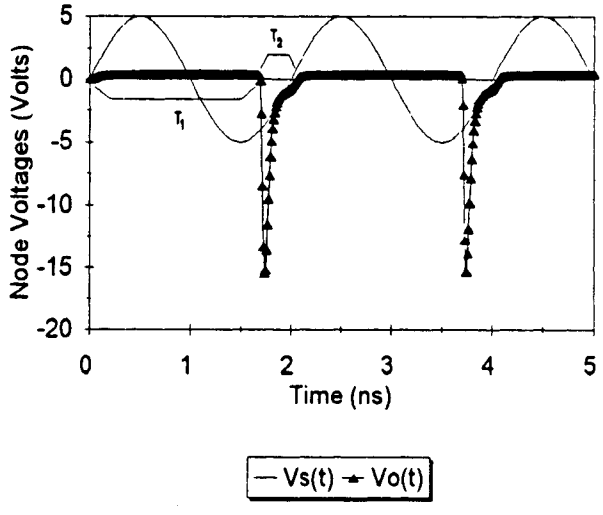

Figure 4.4 SRD Pulse Generator Excitation and Output Voltage Simulation $V_s(t)$ - Excitation Voltage. $V_o(t)$ - Output Voltage. If one period of the excitation voltage is defined as T, then T_1 is the time interval that is part of one cycle in which $V_o(t)$ maintains a DC level of zero volts. T_2 is the time interval of the pulse on $V_o(t)$.

From figure 4.4, each period of the excitation sinusoid can be divided into two intervals. The time interval during which the output voltage remains clamped at a DC level of zero volts will be referred to as T_1 and the remaining time interval will be referred to as T_2. If the period of the excitation sinusoid is defined as T then T can be expressed in terms of T_1 and T_2 by equation (4.2).

$$T = T_1 + T_2 \tag{4.2}$$

The current through the inductor in Fig 4.3 as a function of time is shown in Fig. 4.5.

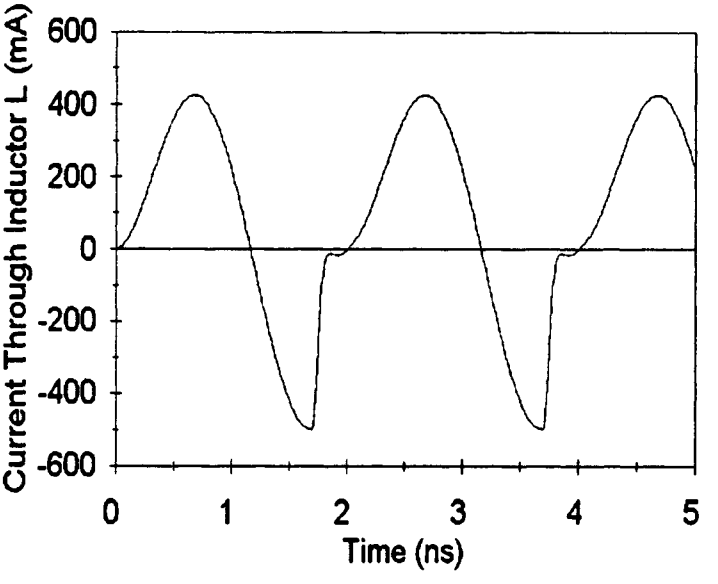

Figure 4.5 Simulation of Current Through SRD Pulse Generator Series Inductor L

During the time interval T_1 the step recovery diode is forward biased and for the purposes of the analytical analysis we will assume that it appears as an infinite capacitance or essentially a short to ground. The equivalent circuit for the time interval

T_1 is given in Fig. 4.6 [17]. It should be noted that during the time interval T_1 the current through the inductor becomes negative which represents the current due to the depletion of the charge that has been stored in the forward biased step recovery diode.

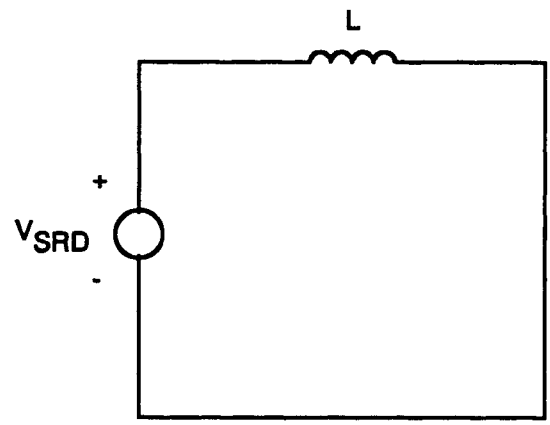

Figure 4.6 Equivalent Circuit of the SRD Pulse Generator During the Time Interval $0 \leq t \leq T_1$.

When the storage time of the step recovery diode is up, the stored charge in the step recovery diode has been depleted and the device turns off quickly. This occurs at the beginning of the time interval T_2 and the equivalent circuit of Fig. 4.7 holds.

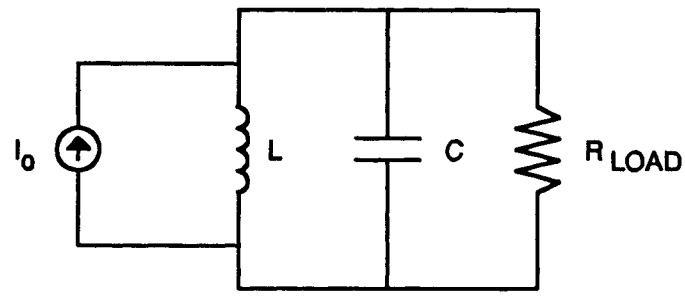

Figure 4.7 SRD Pulse Generator Equivalent Circuit in Effect During the Time Interval $T_1 < t \leq T_2$.

The current through an inductor can be written in terms of the initial current through the inductor which will be defined as I(0) and the integral of the voltage over the time interval of interest.

$$I(t) = I(0) + \frac{1}{L}\int_0^t v dt \tag{4.3}$$

The voltage from the excitation source can be defined as

$$V_{PG}(t) = V_1 \sin(\omega t) + V_{DC} \tag{4.4}$$

A general expression for the current through the inductor as a function of time

is given in (4.5).

$$I(t) = I(0) + \frac{V_1}{L\omega} - \frac{V_1}{L\omega}\cos(\omega t) + \frac{V_{DC}t}{L} \qquad (4.5)$$

When the step recovery diode turns off and becomes reversed biased, the negative current that is flowing through the inductor, which is defined as I_o, cannot change instantaneously and this negative current is the excitation in the resonant RLC circuit of Fig. 4.7. The voltage cross the RLC elements of the circuit of Fig. 4.7 is given by equation (4.6) where the substitution of the time variable t' is made which is defined over the interval T_2.

$$V_o(t') = I_o\left[\frac{4R^2CL}{4R^2C^2 - LC}\right]^{-\frac{1}{2}}\sin\left(\left[\frac{1}{LC} - \frac{1}{4R^2C^2}\right]^{\frac{1}{2}}t'\right)e^{-\frac{1}{2RC}t'} \qquad (4.6)$$

As can be seen from equation (4.6), the response of the SRD pulse generator circuit during the T_2 time interval is a damped sinusoid with a resonance frequency ω_r as shown in (4.7).

$$\omega_r = \left[\frac{1}{LC} - \frac{1}{4R^2C^2}\right]^{\frac{1}{2}} \qquad (4.7)$$

The pulse width of the base of the output voltage pulse T_2 is simply half of the period that corresponds to the resonance frequency.

In practice the assumption that the reverse biased depletion capacitance of the step

recovery diode is a constant is not entirely correct. The actual value of the depletion capacitance would change as a function of the reverse bias voltage.

A simulation of the SRD pulse generator was implemented in PSPICE.

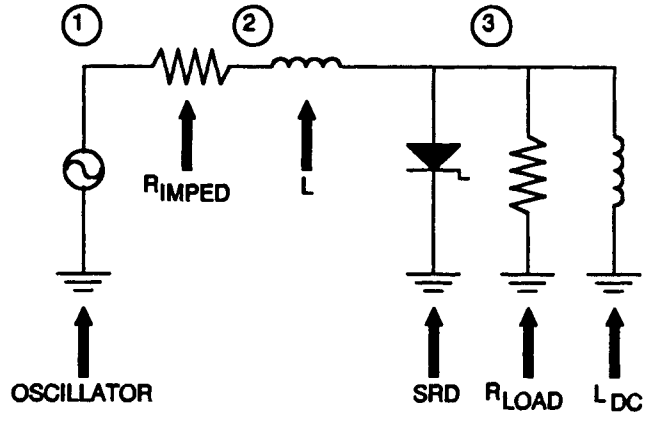

Figure 4.8 PSPICE Step Recovery Diode Circuit Simulation Circuit elements correspond to Fig. 4.3 with the exception of the DC source which is assumed to be 0, LDC which is a DC short to ground that is present in the physical device is represented by a 100 μH inductor, and RIMPED which represents a power tuning resistor. RLOAD is set to 50 Ohms. Oscillator is 500 MHz 5 Volt peak sinusoid. The diode model is a convention PSPICE pn junction diode with parameters:

τ_t	Transit Time	1.9×10^{-9} s
I_x	Saturation Current	10.3×10^{-9} A
C_{j0}	Zero Bias Depletion Capacitance	1.8205 pF
V_j	Built In Voltage	0.6302 V
R_{IMPED}	Series Power Tuning Resistor	9.0 Ω
L	Series SRD Inductor	2.0 nH

The PSPICE model for a convention pn junction diode was used as the step recovery diode in the SRD pulse generator circuit simulation. The PSPICE model for the diode does not have a parameter to specify the turn off time τ_o. Since the PSPICE diode model assumes that when the storage time τ_s elapses, the stored charge is completely depleted, the model simulates an ideal step recovery diode with respect to the turn off time τ_o.

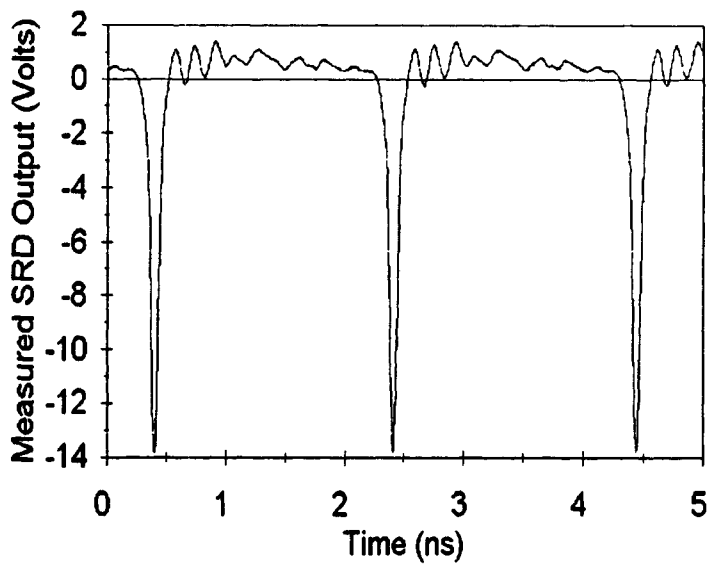

Figure 4.9 Measured SRD Pulse Train Generator Response. Pulse generator is tuned to 500 MHz and is driven into the 50 Ohm load of the scope probe.

The curves of Fig. 4.4 and Fig. 4.5 above were generated with a PSPICE simulation of the step recovery diode circuit of Fig. 4.8. An unwanted feature of the voltage characteristic shown in Fig. 4.4 is visible at the trailing edge of the pulses where there is a short time delay before the voltage returns to its DC value of zero volts. This feature is due to the fact that the base width of the output pulse is not exactly equal to the storage time subtracted from the period of the excitation sinusoid. The experimental results, as shown in Fig. 4.9 above, demonstrate a fairly good agreement between the PSPICE simulation of the SRD output pulse response and the actual measurements taken with a 20 GHz Hewlett Packard digital sampling oscilloscope.

4.3 Conventional SRD Laser Driver

A conventional step recovery diode laser driver can be used to gain switch a laser diode. This method has been used before by Paulus [3] in performing his gain switching experiments. The experimental set up for the conventional SRD driver is shown in Fig. 4.10.

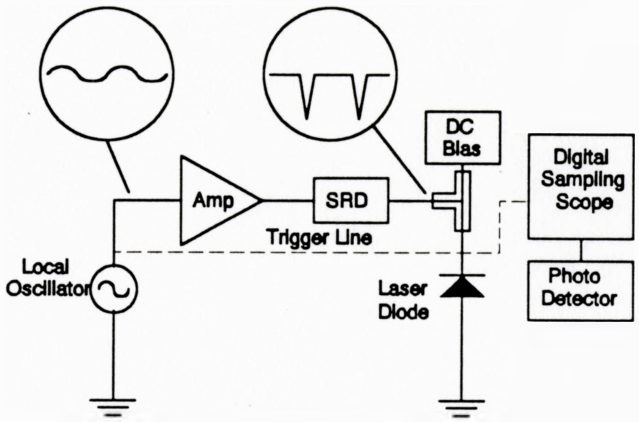

Figure 4.10 Conventional SRD Semiconductor Laser Diode Gain Switching Experiment. Equipment used in this experiment is the same as was listed in Fig. 3.5 of the previous chapter.

Fig. 4.9 shows the time response of a 500 MHz SRD. As expected the repetition rate of the pulse train is 2 ns. We can also observe that the 15 V output amplitude of the pulses correspond to 300 mA of current into a 50 Ohm load. It can also be observed that the FWHM of the electrical pulse is approximately 70 ps. As was discussed in Chapter 3, this pulse width and current amplitude are more than sufficient to gain switch the laser diode.

The conventional SRD driver configuration is simple to implement and exhibits low jitter that is associated with SRD's as per O'Dell [5]. Typical jitter measurements are 3 ps for a conventionally driven SRD pulse generator.

A major drawback of this driver technique is that it does not allow for a variable repetition rate. The frequency to which the SRD pulse generator is tuned is fixed and

therefore the pulse repetition rate will correspond to this frequency and will also be fixed.

4.4 Mono-Cycle SRD Laser Driver

A step recovery diode pulse train generator will respond with an output pulse to a single cycle of the excitation waveform to which it is tuned. If a mono-cycle can be generated that mimics one period of the tuned excitation waveform, than this mono-cycle can be repeated at different repetition rates. The SRD pulse generator that is tuned to a specific frequency will now output a pulse train at the repetition rate of the mono-cycles. The apparatus for this experiment is shown in Fig. 4.11.

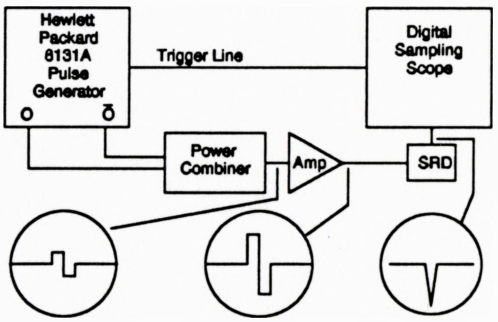

Figure 4.11 Mono-Cycle SRD Experiment Power Combiner is a Mini Circuits ZFRSC-42 splitter/combiner. Amplifier is a Mini Circuits ZHL-1A with a gain of 16 dB and with a bandwidth of 2 MHz to 500 MHz. The step recovery diode pulse generator is a Hewlett Packard 500 MHz device.

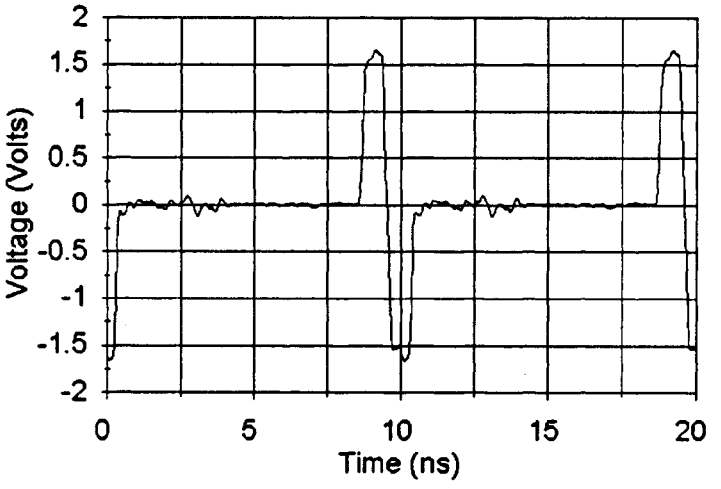

Figure 4.12 Measurement of the Combined Mono-Cycle Waveform. Period of each mono-cycle is 2 ns and the repetition rate of the mono-cycle pulse train is 100 MHz.

In this experiment, Channel A of a Hewlett Packard 8131A pulse generator was configured to output pulses at a 100 MHz repetition rate, an amplitude of 2.50 Volts and a pulse width of 1 ns. Channel B was configured to output an exact replica of Channel A but inverted and delayed in time by 800 ps.

The two pulses are combined through a power combiner resulting in the waveform of Fig. 4.12. This waveform is then amplified resulting in the waveform of Fig. 4.13.

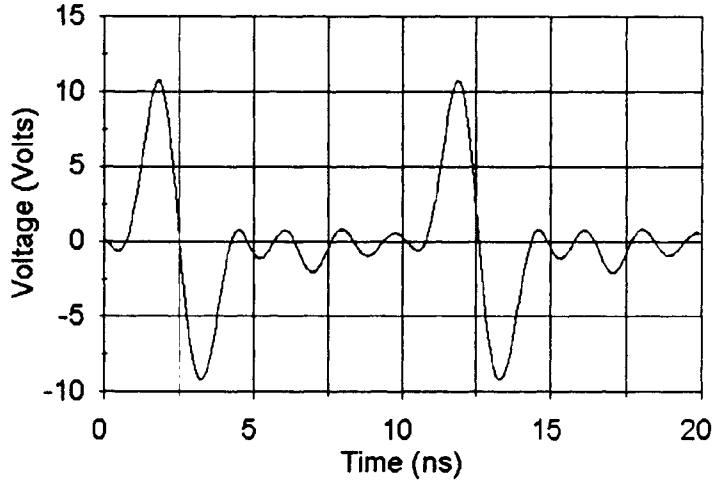

Figure 4.13 Measurement of the Amplified Mono-Cycle Waveform.

The mono-cycle waveform of Fig. 4.13 was then used to excite a 500 MHz tuned SRD pulse generator which responded with the pulse train of Fig. 4.14.

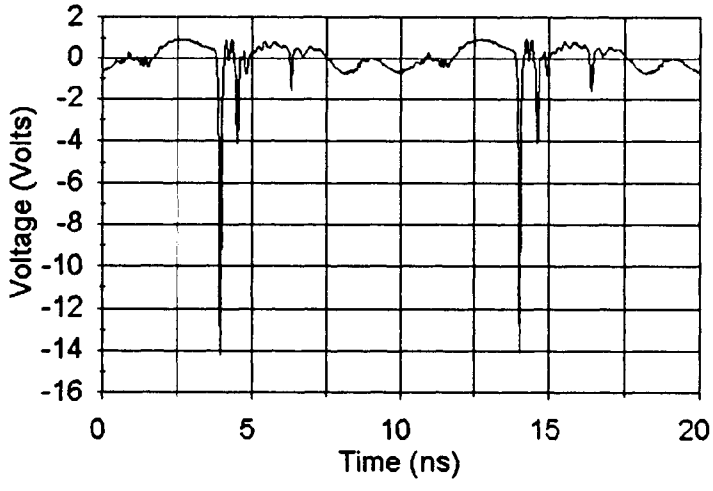

Figure 4.14 Response of the SRD to the Amplified Mono-Cycle Waveform of Figure 4.13.

It can be seen from Fig. 4.14 that the 500 MHz SRD pulse generator which, when driven conventionally, produced a pulse train that repeated every 2 ns could be made to repeat at a 100 MHz repetition rate with a pulse every 10 ns. It can also be seen from Fig. 4.14 that there are some secondary spikes present in the SRD response. These are oscillations caused by the limited 500 MHz bandwidth of the amplifier. The

secondary spiking is not as significant in the 100 MHz SRD response shown in Fig. 4.15 The data in Fig. 4.15 was taken from a 100 MHz SRD that was mono-cycled at 20 MHz.

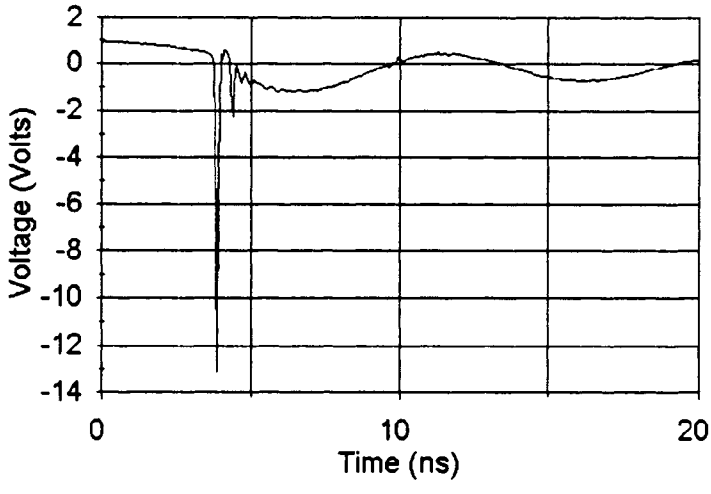

Figure 4.15 Measurement of a 100 MHz tuned SRD Mono-Cycled at 20 MHz. Secondary spiking in the response characteristic is not as severe as the 500 MHz case.

In general there is an increase in jitter associated with the mono-cycle driving technique. For the 100 MHz SRD the jitter increased from 3.0 ps when the SRD was driven in the conventional manner to 5.6 ps when the SRD was mono-cycled. The mono-cycle driver technique allows for a variable repetition rate at the expense of

increased jitter.

4.5 Bias Control SRD Pulse Quenching Laser Driver

In order to gain switch a laser diode, sufficient bias current must be supplied to the device in addition to the excitation current pulse. As was discussed earlier, the device must be biased near the threshold value. Demokan [9] develops an analytical expression for the optimum bias current for gain switching. Demokan also states that in order to achieve optimum gain switching performance, the laser diode should be biased between 90% and 100% of the threshold current. We have observed experimentally that a laser diode can be subjected to continuous pulses from a step recovery diode pulse generator, however the device will not emit gain switched pulses unless sufficient bias current is supplied. With this in mind, a circuit can be conceived of where the bias current is turned on to extract an optical pulse when desired. When the bias is turned off the optical pulses from the laser diode are quenched despite the fact that the SRD continues to pulse. The conceptual block diagram of such a circuit is shown in Fig. 4.16.

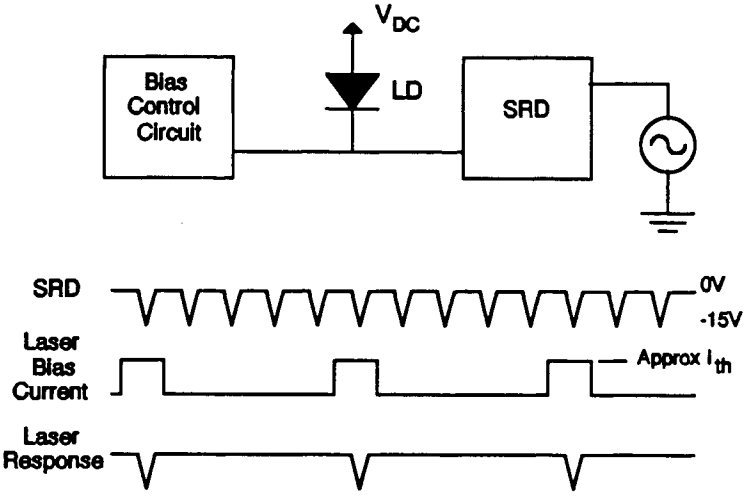

Figure 4.16 Conceptual Block Diagram of Bias Control Optical Pulse Quenching SRD Laser Driver Circuit.

In practice this circuit was implemented with gallium arsenide field effect transistors (GaAs FETs) which were used to control the bias current through the laser diode. The actual circuit that was implemented is shown in Fig. 4.17. The transistors used in this experiment were NEC's NE76038 MESFETs.

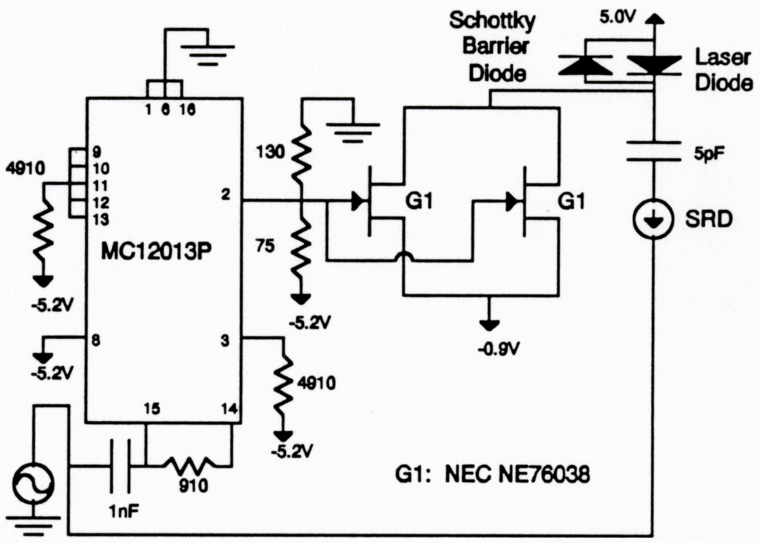

Figure 4.17 Circuit Diagram of Bias Control Optical Pulse Quenching SRD Laser Driver Circuit.

As can be seen in Figure 4.17, the laser diode sits at the drain of the transistors as does the step recovery diode. The source of the GaAs FETs were biased at -0.9 V because -0.9 V corresponds to an ECL logic high signal.

With this biasing arrangement an ECL logic output can be connected to the gates of the transistors. When the ECL logic level is high, the gate to source voltage of the GaAs FETs will be V_{gs} = 0.0 V. A large current will flow through the transistors which will supply a bias current of approximately the threshold value to the laser. When the logic level is low or at -1.7 V, the gate to source voltage V_{gs} = -0.8 V. In this case

practically no current will flow through the transistors and the laser will have essentially no bias current thus quenching the optical pulses.

The experimental apparatus is shown in Fig. 4.18.

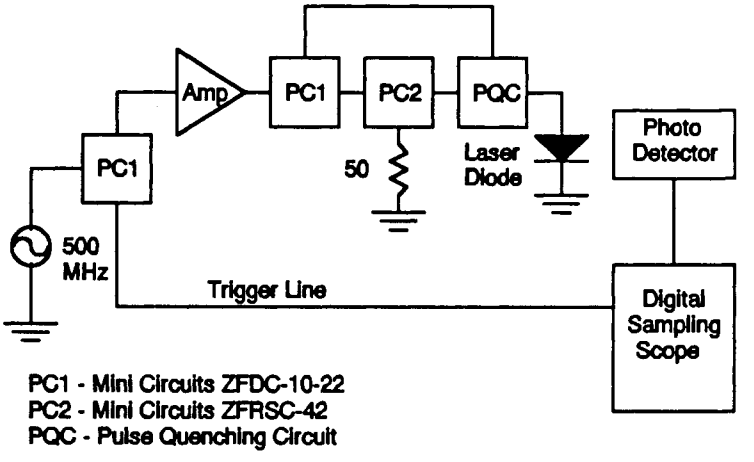

Figure 4.18 Experimental Apparatus for the Bias Control Optical Pulse Quenching SRD Laser Driver Circuit.

A 500 MHz oscillator was used to drive a tuned 500 MHz SRD pulse train generator and an ECL divide by 10 prescalar chip MC12013P by Motorola. The prescalar divides the 500 MHz signal down to 50 MHz which drives the gates of the GaAs FETs. The response from the laser should consist of a series of optical pulses

during the half of the period for which the ECL logic level of the prescalar is high. For the other half of the periodic ECL waveform there should be an absence of optical pulses. We can see from Fig. 4.19 that this is in fact what is observed experimentally.

This circuit can be used to switch in an optical pulse when required using ECL level signals. If the pulse repetition frequency is 100 MHz, then every tenth pulse could be switched in resulting in a 10 MHz pulse train.

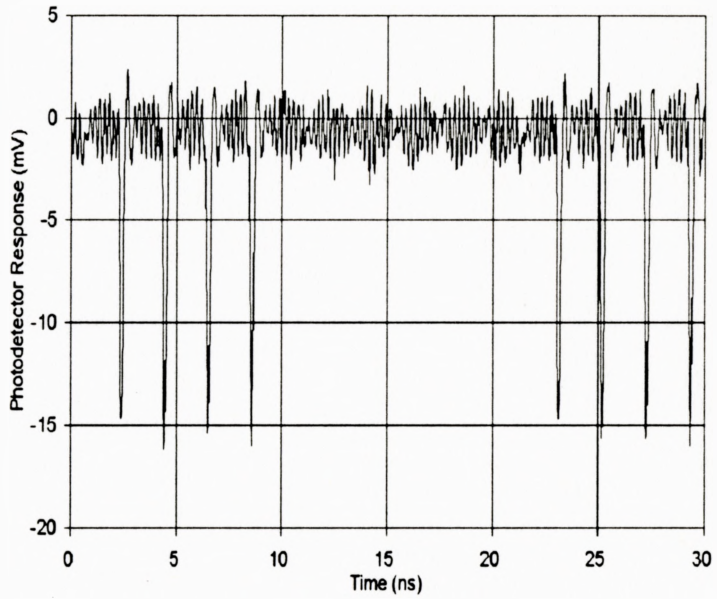

Figure 4.19 Photodetector Response from the Optical Output of a Semiconductor Laser Diode Driven with the Bias Control Optical Pulse Quenching SRD Laser Driver Circuit of Fig. 4.17.

4.6 Integrated Spice Simulation of the Optical Pulse Quenching Circuit

The circuit shown in Fig. 4.17 can be simulated in PSPICE, with some simplifications, together with the laser diode model discussed in Chapter 2. The simulated circuit is shown in Fig. 4.20.

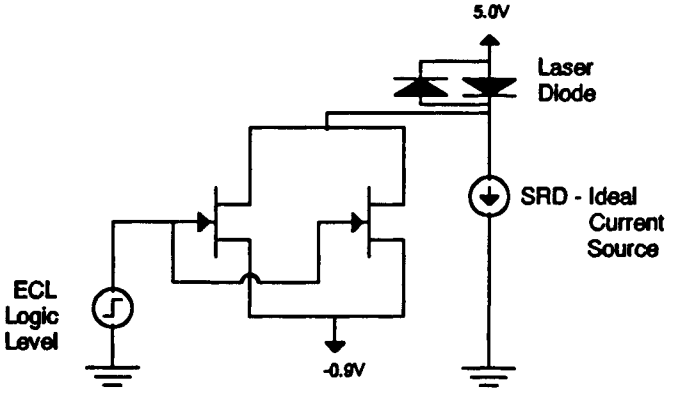

Figure 4.20 PSPICE Simulation Circuit of the Bias Control Optical Pulse Quenching SRD Laser Driver Circuit of Fig. 4.17.

The PSPICE simulation results of the optical output from the laser diode are shown in Fig. 4.21.

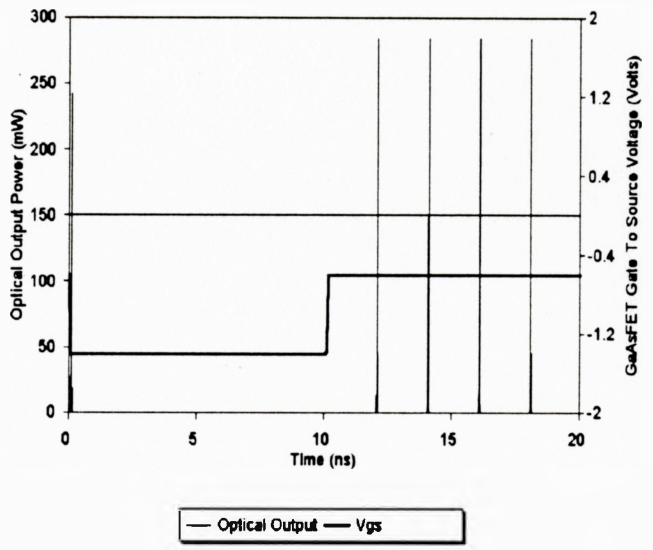

Figure 4.21 PSPICE Simulation of the Circuit of Figure 4.20. Laser Driver equivalent circuit optical response is shown along with the bias control modulation gate to source voltage on the GaAs FETs.

As can be seen in Fig. 4.21, the optical output bears the same qualitative features as the results that were observed experimentally in Figure 4.19 in that the simulation predicts the optical pulse quenching characteristics of the laser driver circuit.

4.7 Comparison of Gain Switched Laser Driver Circuit Techniques

The table below compares the principal features of various gain switched laser

driver techniques that have been studied. Although the conventional SRD laser driver exhibits the lowest timing jitter, its frequency is fixed and it does not provide the option of a triggered pulse. The mono-cycle SRD generator has been tested in various forms. The first of which was where the mono-cycles were generated by the HP 8131A pulse generator. The timing jitter observed from this version of the mono-cycle pulse generator exhibits a slight increase in timing jitter over the conventional SRD laser driver. Mono-cycles can also be generated by differentiating an ECL level signal with a simple RC differentiator network. Unfortunately although extremely simple, this technique exhibits the highest timing jitter of all the methods investigated. Both mono-cycle driver techniques have the desirable characteristics of supplying a pulse from the SRD that can be triggered on demand. The frequency of the pulse train produced by the mono-cycle SRD drivers is variable.

Laser Driver	**Variable Frequency**	**Triggered Pulse**	**Timing Jitter**
Conventional SRD Laser Driver	No	No	3.1 ps
Mono-Cycle	Yes	Yes	5.6 ps

Mono-Cycle (RC)	Yes	Yes	20.9 ps
Bias Control * Pulse Quencher	Yes	No	13 ps

*** Optical**

The bias control pulse quencher circuit exhibits 13 ps jitter however it must be noted that unlike the other jitter measurements quoted in the table above, the pulse quencher jitter measurement is of the optical not the electrical pulse. This circuit allows for the facility of generating a variable frequency pulse train by switching in an optical pulse when required. In the strictest sense of the concept the circuit does not provide a triggered pulse on demand since the SRD pulses continuously and the optical pulses are switched in and out by means of controlling the DC bias current through the laser diode.

Conclusion

In this thesis two novel techniques for gain switching a semiconductor laser diode have been presented. The first technique involved a novel bias control scheme in which the bias to a semiconductor laser diode, that was driven with an SRD, was turned on and off in order to switch the optical pulses in and out as desired. A prototype circuit for the bias control laser driver was implemented and it was discovered that the circuit functioned as expected. The second technique investigated was one in which the step recovery diode pulse train generator was mono-cycled to produce variable repetition rate current pulses that could be used to gain switch a semiconductor laser diode. It was discovered that mono-cycling of the step recovery diode pulse train generator added a nominal amount of jitter to the output electrical pulse over and above the jitter that was observed when the SRD was driven in a conventional manner.

An equivalent circuit of the semiconductor laser diode was implemented in PSPICE in an attempt to qualitatively model the interaction of the electronic components of the laser driver circuit with the semiconductor laser diode. The equivalent circuit model was benchmarked against analytically derived solutions to the semiconductor laser

diode rate equations for DC, AC and gain switched transient excitation. It was discovered that there was good agreement between the analytically derived rate equation solutions and the predictions of the equivalent circuit model simulations for the DC and AC excitation case. For the gain switched transient excitation case there was good agreement between the simulated laser diode equivalent circuit model response and the analytically calculated response of the pulse width and optical pulse delay characteristics. A qualitative agreement was found to exist between the measurements of the laser diode terminal voltage response and the PSPICE simulation of the laser diode terminal voltage for the gain switching experiment. The laser diode equivalent circuit model also predicted a 30-35 ps pulse width for the gain switching experiment which agreed with the measured pulse width.

Future Research Possibilities

Having verified the feasibility of mono-cycling the step recovery diode pulse generator circuit, there exists the possibility of developing a dedicated circuit to mono-cycle the SRD pulse generator.

A quantitative assessment of the laser diode equivalent circuit model's ability to predict the optical and electrical response of the device could only be undertaken if the rate equation parameters for the device being simulated were readily available.

Measurement techniques for some of these parameters remains the subject of research [18]. The model could be enhanced to include such effects as Auger recombination relatively easily.

Appendix A Derivation of the Laser Diode Equivalent Circuit Model Electrical Current Component Equation

In this appendix, the equation for the laser diode equivalent circuit electrical current components is derived. First it is necessary to establish the dimensional convention to be used in the derivation.

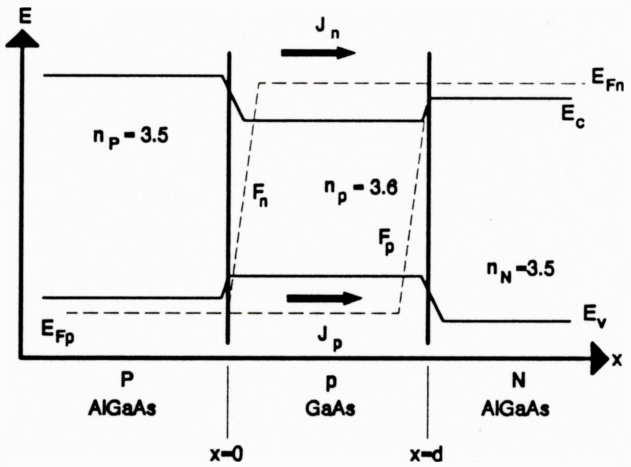

Figure A.1 PpN Laser Diode Energy Band Diagram Under Forward Bias F_n - Electron Quasi-Fermi Level. F_p - Hole Quasi-Fermi Level. E_{FP} - Equilibrium Fermi Level p type AlGaAs. E_{FN} - Equilibrium Fermi Level n type AlGaAs. η_P - P AlGaAs Index of Refraction. η_p - p GaAs Index of Refraction. η_N - N AlGaAs Index of Refraction.

The positive x direction is taken as the reference direction. All integrations are performed with respect to the reference direction. All limits on the respective integrals are established based on the direction of the minority carrier flow. Signs of the resultant derived equations are interpreted in terms of the reference direction.

It should be remembered that it has been assumed that the minority carrier densities are not a function of position in the active region for 0 < x d. There is assumed to be no minority carrier current flow across the respective energy barriers at x=0 for electrons and x=d for holes. In essence it is assumed that at x=0, the total current density is being carried by the minority carrier holes and at x=d the total current density is being carried by the minority carrier electrons.

If one examines the flow of minority carrier electrons across the Np heterojunction then it becomes clear that the flow is in the negative x direction. The minority carrier diffusion equation for electrons as defined by Pierret [13] is shown below.

$$\frac{1}{q}\frac{\partial J_n(x,t)}{\partial x} = \frac{n(t)}{\tau_{ns}} + \frac{\partial n(t)}{\partial t}$$

The spatial dependence on x of the minority carrier diffusion equation for electrons can be integrated out as shown below.

$$\int_{d}^{0} \frac{\partial J_n(x,t)}{\partial x} dx = \int_{d}^{0} \frac{qn(t)}{\tau_{ns}} dx + q\frac{\partial}{\partial t}\int_{d}^{0} n(t)dx$$

The above equation can be written as

$$J_n(0,t) - J_n(d,t) = -\frac{qn(t)d}{\tau_{ns}} - qd\frac{\partial n(t)}{\partial t}$$

Since it has all ready been assumed that at x=0 the entire current density is being carried by the minority carrier holes, $J_n(0,t)=0$. All the remaining terms on both sides of the equation can be multiplied by the area A in order to write the equation in terms of current. What results is simply the equation for I_e of (2.28).

$$i_n(t) = \frac{qdAn(t)}{\tau_{ns}} + qdA\frac{dn(t)}{dt}$$

The first term represents the spontaneous emission current component and the second time differential term represents the charge storage current component.

Appendix B Gaussian Pulse Deconvolution Formula Derivation

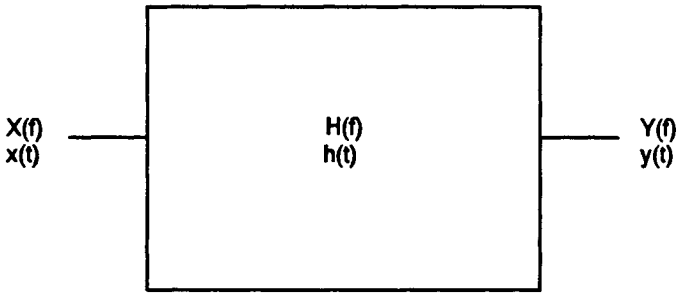

$$H(f) = \frac{Y(f)}{X(f)}$$

Figure B.1 Block Diagram of System with Transfer Function H(f), Input X(f) and Output Y(f).

In this appendix an analytical formula is derived for the deconvolution of a system impulse response h(t), from the output response in time y(t). The derivation assumes that the input to the system x(t) is a gaussian pulse and that the impulse response h(t) of the system is gaussian. This formula is useful when deconvolving the pulse broadening effect of the photodetector from the measurement of the detector response to input light pulses.

For the system block diagram above, the H(f) and X(f) are gaussian functions of frequency defined as shown below.

$$H(f) = \frac{1}{\sqrt{2\pi\sigma_1^2}} e^{-\frac{f^2}{2\sigma_1^2}}$$

$$X(f) = \frac{1}{\sqrt{2\pi\sigma_2^2}} e^{-\frac{f^2}{2\sigma_2^2}}$$

The output Y(f) can be derived using the relations Y(f) = H(f) X(f).

$$Y(f) = \frac{1}{2\pi\sigma_1\sigma_2} e^{-\left(\frac{1}{2\sigma_1^2} + \frac{1}{2\sigma_2^2}\right)f^2}$$

The Fourier pair of interest in this example is

$$e^{-\pi\frac{t^2}{t_o^2}} \rightharpoonup t_o e^{-\pi t_o^2 f^2}$$

Thus

$$2\pi t_o^2 = \left(\frac{1}{\sigma_1^2} + \frac{1}{\sigma_2^2}\right)$$

$$\frac{1}{t_o^2} = 2\pi\left(\frac{1}{\sigma_1^2} + \frac{1}{\sigma_2^2}\right)^{-1}$$

$$\frac{\pi}{t_o^2} = 2\pi^2\left(\frac{1}{\sigma_1^2} + \frac{1}{\sigma_2^2}\right)^{-1}$$

Where $\Sigma = 1/\sigma$

$$\frac{\pi}{t_o^2} = \frac{2\pi^2}{\Sigma_1^2 + \Sigma_2^2} = \frac{2\pi^2}{\Sigma_3^2}$$

Therefore

$$\Sigma_3^2 = \Sigma_1^2 + \Sigma_2^2$$

The expression for the full width half maximum pulse width of a gaussian pulse is

$$\tau_{FWHM} = \sqrt{8\Sigma^2 \ln(2)}$$

Therefore the desired result is

$$\tau_3^2 = \tau_1^2 + \tau_2^2$$

Bibliography

[1] New G.H.C., and D. Wood, "Dynamics of gain-switched and model-locked semiconductor lasers," Journal of Modern Optics, vol. 38, no. 4, pp. 785-799, 1991.

[2] Galvanauskas A., "Ultrafast Optoelectronics with Semiconductor Laser Diodes," Royal Institute of Technology, Department of Physics II, Stockholm, Sweden, 1992, TRITA-FYS 2113.

[3] Paulus P., R. Langenhorst, and D. Jager, "Generation and optimum control of picosecond optical pulses from gain-switched semiconductor lasers," IEEE Journal of Quantum Electronics, vol. 24, no. 8, pp. 1519-1523, Aug. 1988.

[4] Garside B.K., and R.E. Park, "Ultrashort pulses from semiconductor diode lasers," Optical Laser Technology, vol. 15, pp. 91-94, Apr. 1983.

[5] O'Dell T.H., Circuits for Electronic Instrumentation, Cambridge University Press, New York, 1991.

[6] Tucker R.S., "Large-signal circuit model for simulation of injection-laser modulation dynamics," IEE Proc., vol. 128, pt. I, no. 5, pp. 180-184, Oct. 1981.

[7] Habermayer I., "Nonlinear circuit model for semiconductor lasers," Optical and Quantum Electronics, vol. 13, pp. 461-468, 1981.

[8] Jones Jr. W.B., Introduction to Optical Fiber Communication Systems," Holt, Rinehart and Winston, Toronto, 1988.

[9] Demokan M.S., and A. Nacaroglu, "An analysis of gain-switched semiconductor lasers generating pulse-code-modulated light with a high bit rate," IEEE Journal of Quantum Electronics, vol. 20, no. 9, pp. 1016-1022, Sept. 1984.

[10] Yariv A., Optical Electronics, Holt, Rinehart and Winston, Toronto, 1991.

[11] Streetman B.G., Solid State Electronic Devices, Prentice Hall, New Jersey, 1990.

[12] Cheo P.K., Fiber Optics & Optoelectronics, Prentice Hall, New Jersey, 1990.

[13] Pierret R.F., Advanced Semiconductor Fundamentals, Volume VI Modular Series on Solid State Devices, Addison-Wesley, Don Mills, 1987.

[14] Tucker R.S., "Circuit model of double-heterojunction laser below threshold," Proc. IEE, vol. 128, pt I, no. 3, pp. 101-106, June 1981.

[15] Elkadi H., J.P. Vilcot, S. Maricot, and D. Decoster, "Microwave circuit modeling for semiconductor lasers under large and small signal conditions," Microwave and Optical Technology Letters, vol. 3, no. 11, pp. 379-382, Nov. 1990.

[16] Moll J. L., S. Krakauer, and R. Shen, "P-N junction charge-storage diodes," Proc. IRE, vol. 50, pp. 43-53, 1962.

[17] Maas S., Nonlinear Microwave Circuits, Artech House, 1988.

[18] Zou Y., J.S. Osinski, P. Grodzinski, P.D. Dapkus, W.C. Rideout, W.F. Sharfin, J. Schlafer, and F.D. Crawford, "Experimental study of Auger recombination, gain and temperature sensitivity of 1.5 μm compressively strained semiconductor lasers," IEEE Journal of Quantum Electronics, vol. 29, no. 6, pp. 1565-1574, June, 1993.